FLUORESCENCE CORRELATION SPECTROSCOPY TO MEASURE MEMBRANE PERTURBATIONS THAT AFFECT RECEPTOR-MEDIATED SIGNALING

A Thesis

Presented to the Faculty of the Graduate School

of Cornell University

In Partial Fulfillment of the Requirements for the Degree of

Master of Science

by

Robert Palmere

May 2018

ABSTRACT

Diffusion constants (D) and transient confinement times (τ_0) of membrane bound fluorescent probes thought to partition into liquid-ordered (L_o) or liquid-disordered (L_d) inner / outer leaflet membrane regions were measured by imaging fluorescence correlation spectroscopy. Resting rat basophilic leukemia cells were used under a variety of pharmacological perturbations. Yellow Fluorescent Protein-Glycan-Glycosylphosphatidylinositol (YFP-gl-GPI)was used as the outer-leaflet L_o-like region marker, palmitoyl and myristoyl-Enhanced Green Fluorescent Protein (PM-EGFP) was used as the inner-leaflet L_o-like region marker, and geranylgeranylated EGFP (EGFP-GG) was used as an L_d-like lipid region marker on the inner leaflet. Treatments included C2- & C6-ceramide, cholesterol depletion by methyl-beta-cyclodextrin, 7-ketocholesterol addition, and cytochalasin D. These membrane perturbing treatments were done in efforts to identify a condition in which L_o-like regions would be disrupted for further study regarding IgE high affinity receptor signaling. C6-ceramide treatments showed a propensity to disorder L_o-like regions symmetrically for both leaflets of L_o-like domain markers, but only resulted in a ~10% decrease in τ_0 for Alexa488-IgE-FcεRI without significant change in D. Aside from short-chained ceramide treatment, all other treatments resulted in either no change, or some degree of increase in τ_0 for these fluorescent reporters, indicating the local lipid environment as not having changed or increased respectively. Asymmetric effects under treatment conditions between lipid monolayer L_o-like preferring markers were also observed.

BIOGRAPHICAL SKETCH

Robert Palmere was born on October 23, 1993 in Livingston, New Jersey to Daniel and Michele Palmere. He is second of two children, the other being his brother Alan. His interest in the natural world stems from observing insects as a young child. It was not until his sophomore year while attending Seton Hall University that he discovered his interest in Chemistry. He graduated Magna Cum Laude from Seton Hall University in 2016 with a Bachelor of Science degree in Biochemistry and a minor in Applied Scientific Mathematics. In August of 2016, Robert began his graduate studies at Cornell University in Ithaca, New York. After being introduced to the intriguing work being conducted in the laboratory of Dr. Barbara Baird and Dr. Dave Holowka, he has decided to pursue his interest on cell membranes and, as a result, has produced this body of work. Robert has been accepted to other universities as a PhD candidate and plans to earn his PhD in the immediate coming years.

ACKNOWLEDGMENTS

I would like to thank all those who have made this work possible. I would especially like to thank:

- Dr. Barbara Baird and Dr. David Holowka for the opportunity to conduct research under their advisement and without whose assistance this thesis would not have come to fruition

- Dr. Nirmalya Bag for his mentorship throughout my time at the Baird-Holowka laboratory and for his hands-on guidance during sample preparations

- Dr. Jeremy Baskin and Dr. Warren Zipfel for serving on my committee

- My father, mother and brother for their love and support

TABLE OF CONTENTS

TABLE OF FIGURES

LIST OF TABLES

LIST OF EQUATIONS

LIST OF ABBREVIATIONS

7-KC	7-Ketocholesterol
ACF	Autocorrelation Function
CytoD	Cytochalasin D
DMEM	Dulbecco's Modified Eagle Medium
DMIRB	Leica DMIRB Inverted Confocal Microscope
DMSO	Dimethyl sulfoxide
DNP	2,4-dinitrophenyl
DOPC	1,2-dioleoyl-sn-glycero-3-phosphocholine
DOPE	1,2-dioleoyl-sn-glycero-3-phosphoethanolamine
DPPC	Dipalmitoylphosphatidylcholine
DRM	Detergent Resistance Membrane
ECM	Extracellular Matrix
EDTA	Ethylenediaminetetraacetic Acid
EGFP	Enhanced Green Fluorescent Protein
EGFP-GG	Enhanced Green Fluorescent Protein – Geranylgeranyl
EMCCD	Electron Multiplying CCD (Charge Coupled Device) Camera
FCS	Fluorescence Correlation Spectroscopy
FLIM-FCS	Fluorescence-Lifetime Imaging Microscopy - FCS
GUV	Giant Unilamellar Vesicle
FBS	Fetal Bovine Serum
FRAP	Fluorescence Recovery After Photobleaching
FRET	Förster Resonance Energy Transfer
GFP	Green Fluorescent Protein
GG	Geranylgeranyl
GPI	Glycosylphosphatidylinositol
HPLC	High Performance Liquid Chromatography
IFCS (ITIR-FCS)	Imaging FCS (Imaging Total Internal Reflection - Fluorescence Correlation Spectroscopy
IgE	Immunoglobulin E
ITAM	Immunoreceptor Tyrosine-based Activation Motif
Lat-A	Latrunculin-A
LUV	Large Unilamellar Vesicle
Lyn-EGFP	Lyn-kinase-EGFP
MβCD	methyl-β-cyclodextrin
MD	Molecular Dynamics (e.g. MD simulations)
PC	Phosphatidylcholine
PE	Phosphatidylethanolamine
PI	Phosphatidylinositol
PM	palmitoyl and myristoyl
PS	Phosphatidylserine
RBL	Rat Basophilic Leukemia
SLB	Supported Lipid Bilayer
SM	Sphingomyelin
TIR	Total Internal Reflection
TIRF	Total Internal Reflection Fluorescence
ULV	Unilamellar Vesicle
YFP-gI-GPI	Yellow Fluorescent Protein-Glycan-Glycosylphosphatidylinositol

INTRODUCTION

The plasma membrane of a cell exists as a boundary between a cell's internal and external environment and plays a critical role in cellular functions. As the primary barrier separating external and internal environment of a cell, the plasma membrane also acts as a gatekeeper for information exchange via bioactive molecules due to its selective permeability. Hence, the plasma membrane is a cell's first line of defense against external changes and facilitates first-response mechanisms relevant to cell insusceptibility to changes in its external environment. Due to this variety in function, the plasma membrane must be dynamic enough to allow for selective change coinciding with external factors, but if its chemical composition is altered then it must be compensated for in order to remain an active barrier.

Eukaryotic membranes consist of a lipid bilayer which holds implanted biomolecules, including various proteins and carbohydrates. Proteins which are associated with the lipid bilayer can be integral or attached via a lipid anchor (Karp, 2010). The lipid bilayer itself is amphipathic and encompasses hydrophobic acyl chains each with their respective hydrophilic phosphate head group which oppose each other with their hydrophobic fatty acid tails facing inward to each other and hydrophilic head groups facing outward towards the cell's environment and cytosolic interior respectively. This organization forms two leaflets of lipid monolayers, and it is the combination of hydrophilic phosphate head groups and hydrophobic tail interactions that provides the thermodynamic and electrostatic basis for barrier formation. Although there are a variety of lipids which compose the lipid bilayer with the primary being glycerol based lipids, there are two others worth placing emphasis on due to their ubiquity on the plasma membrane: sterols and sphingolipids.

The understanding of biological membranes as having a two-dimensional matrix of phospholipids is consistent with the proposal of the fluid mosaic model by Singer and Nicolson in 1972 (Singer & Nicolson 1972). However, subsequent developments have increased our awareness of a dynamic plasma membrane *in-vivo* significantly. Of key importance to these developments is the recognition of membrane heterogeneity / asymmetry and its importance in live cells. Along with the variety in lipids constituting the plasma membrane, there exists heterogeneity between and within phospholipid monolayers of the outer and inner leaflet portions of the lipid bilayer (Fadeel & Xue, 2009). This heterogeneity / asymmetry manifests itself in a variety of ways including phase behavior, registration of lipid bilayer inner and outer leaflets, and biochemical constituents imbedded between the inner and outer leaflets of the bilayer among others (Marquardt, Geier, & Pabst, 2015).

BILAYER LATERAL HETEROGENEITY

The lateral heterogeneity of lipid monolayers can be understood through examination of each constituent's inherent physical properties. The category of glycerophospholipids includes lipids such as phosphatidylcholine (PC), which composes more than 50% of plasma membrane (Meer, Voelker, & Feigenson, 2008). Glycerophospholipid structure can be generalized as having a glycerol ester attached at C-1 and C-2 to two fatty acid chains and C-3 being attached by a phosphodiester bond which is also attached to a head group. The ester carbonyl bond attaching fatty acid chains are not symmetrical in that the C-2 fatty acid is often unsaturated containing one cis-isomerization at a particular carbon along the chain. Sphingolipids, or, more revealingly named, glycosylceramides, differ from

glycerophospholipids in their saturated (trans-) fatty acid chains. The sphingosine base, which is generally 18 carbons long, contains a trans- conformation double bond at its C-4,5 bond and is bound to its saturated fatty acid chain through an amide bond.

Cholesterol, is distinctive in its lack of long acyl chains, but rather contains three hexane and one pentane rings to form a tetracyclic fused ring. At carbon 3 there exists a hydroxyl group and opposing it lies an iso-octyl carbon chain located at C-17. Cholesterol is vital to cell viability and is mostly concentrated at the plasma membrane highlighting its significance (Lange, et al., 1989).

Of primary importance to the understanding of phase behavior, and therefore the lateral heterogeneity thereby induced between these three classes of lipids that coexist on the plasma membrane, is the packing efficiency, which is dictated by their phosphate headgroups and acyl chain conformations (i.e. degree of saturation). Glycerophospholipids experience low melting temperature (T_m) due to their inefficient packing of unsaturated acyl chains. They exist as a distribution of molecules in fluid phase, which can be categorized as liquid-disordered (L_d) at room temperature (Feigenson, 2009).

Glycosylceramides and other phospholipids containing saturated, long acyl chains exist primarily in liquid-ordered or L_o-like phase on the plasma membrane *in-vivo* (Munro, 2003). The liquid-ordered phase is consists of phospholipids with saturated acyl chains or at most one cis-double bond per phospholipid (Fridricksson et al., 1999) and therefore exhibits decreased packing efficiency and reduced van-der-Waals and hydrophobic interactions thus permitting more lateral movement.

The physical properties inherent to L_o and L_d phases on the plasma membrane are opportune for studying membrane heterogeneity on the plasma membrane *in-vivo* as they provides means of measuring differences experimentally. For instance, let's consider a lipid bilayer with two phases rigidly segregated (ignoring any entropic expenditure) at a fixed temperature. If one is able to measure the displacement of these particular lipids, and the rate of their displacement, then one would be able to gain insight into the phase of which each lipid constituent is rendered at. Hence, fluidity of the lipid bilayer is important to our understanding of the plasma membrane where these two phases can co-exist. The co-existence of L_o and L_d in strictly segregated regions of the membrane is not physiologically relevant, but illustrates the opportunity for experimental inquiry. Eukaryotic cells exhibit a mixing of these two phases at physiological conditions and temperatures. This brings us to the role of cholesterol which is pertinent to the investigative objectives of this thesis.

The structure of cholesterol is predominantly planar due to its tetracyclic backbone being in trans- configuration while its carbon chain at C-17 remains relatively flexible. Just as above, its chemical structure dictates its sterol-lipid interactions on the plasma membrane. Insertion of cholesterol perpendicular to the axis of the plasma membrane which exhibits planarity results in orientation of its hydroxyl group toward the extracellular matrix (ECM) (aqueous solution interface) and the phosphate head groups of neighboring lipids due hydrogen bonding. Hence, cholesterol's tetracyclic backbone does not reside within the base of the opposing acyl chains of its lipid neighbors which constitute the lipid bilayer but rather between C2-C10 of acyl chains as shown by previous NMR data (Vist & Davis, 1990). Cholesterol interactions, just as its lipid counter-parts, largely depend on the degree of saturation of which it is imbedded. Cholesterol's all trans-carbon ring structured backbone has

a large degree of favorable van-der-Waals and hydrophobic interactions with saturated acyl chains of glycerophospholipids such as phosphatidylcholine (PC). The cis-conformation which is characteristic of sphingolipids and unsaturated glycerophospholipids such as DOPC effects cholesterol packing efficiency and results in a dampening of their hydrophobic effect on cholesterol. Rather, the conformational mis-match of cis-conformations rendering kinks in their acyl chains can lead to cholesterol exclusion (Pasenkiewicz-Gierula et al., 1991). In regards to phase heterogeneity on the plasma membrane, cholesterol's critical role is found in its ability to form a new phase with its surrounding lipids. This new phase, named liquid-ordered (L_o) phase, is not found when examining phase behavior of monolayers of single lipid constituents previously named. This new L_o phase can be abstracted as an intermediate phase between gel and L_d depending upon the molar ratio of cholesterol and lipid constituents in these two phases. This intermediate effect induced by cholesterol is the combination of two differing effects on gel and L_d domains (Chen et al., 2007). While cholesterol has a fluidizing effect on gel-like domains, it has a packing effect on lipids that compose liquid-disordered regions (Schwille et al., 2003). This allows for the L_o phase to be founded on tightly packed interactions while enabling increased lateral mobility. The physiological relevancy of cholesterol content results in a junction between L_o and L_d phase at intermediate temperatures. This provides the cell with adaptability to its membrane dynamics from external sources (i.e. semi-permeable) while remaining rigid enough to maintain the established barrier.

DIFFUSION IN PLASMA MEMBRANE

The fluidity of the plasma membrane is of particular interest in regards to measurement of membrane dynamics due to the presence of such heterogeneity. Both lipids and proteins

can undergo different types of diffusion which include translational diffusion, rotational diffusion, and flip-flopping from one lipid monolayer to the other. With these types of diffusion in mind one can narrow the scope of interest to lateral (translational) diffusion due to two important factors. Of first and foremost importance is the biological significance of lateral mobility for proteins residing on the membrane. As proteins diffuse laterally, they interact and diffusion rate can enable or disable a protein from specific sites of signaling (Hoek, et al., 2000). The second factor is that the flip-flopping of proteins or lipids is relatively rare and often requires enzymes (such as flipase) to catalyze this reaction to overcome the activation energy produced by the lipid bilayer itself (Goñi et al., 2010).

As diffusivity of proteins has implications for cell signaling, it is important to recognize the factors that can control diffusion of a protein on a lipid bilayer. These factors include temperature, degree of saturation of surrounding lipid acyl chains, and the composition of the membrane (i.e. protein density, protein-lipid / protein-protein interactions etc.). The understanding that the plasma membrane exhibits lateral fluidity was first introduced by Frye and Eddin in 1970 (Frye & Edidin, 1970). Since then a discrepancy has been uncovered between measured diffusion on model systems in-vitro and slower diffusion measured on the live cell plasma membrane by approximately two orders of magnitude (Lee et al., 1993; Schmidt et al., 1999). The plasma membrane in-vivo exhibits structural differences with those of model in-vitro systems which act to perturb diffusion rates of lipids or proteins laterally. In order to rectify these differences, the following models describing plasma membrane heterogeneity have been proposed which may not be mutually exclusive.

BILAYER LATERAL HETEROGENEITY - RAFT MODEL

The significance of membrane heterogeneity was brought to light over a decade ago with the advent of the “lipid raft” hypothesis supported by experimental evidence of detergent resistant regions of the plasma membrane (Brown & London, 1997). A proper definition of lipid rafts was decided on at the “Keystone Symposium on Lipid Rafts” held on March 23-28th, 2006 which is that “rafts are small 10-200 nm, heterogeneous, highly dynamic, sterol- and sphingolipid-enriched domains that compartmentalize cellular processes.” (Pike, 2006) This model essentially describes the plasma membrane as a dynamic “sea” composed of unsaturated phospholipids in fluid phase which contains nanoscopic “rafts” or segments of L_o phase laterally segregated from the surrounding disordered phase. This functionally based, lateral organization was predominantly discovered by analysis of detergent resistance membranes (DRMs) and therefore has outlined the biochemical constituents thought to be present in such regions. Brown and Rose found that glycosylphosphadtidyl inositol (GPI) anchored proteins, found on the apical membrane surface, are resistant to low density non-ionic detergent (Triton X-100) at low temperature (0° C) (Brown & Rose, 1992). Whereas, later studies have shown these regions to be enriched in cholesterol and sphingolipids (Mayor & Rao, 2004). However, this supporting biochemical evidence and the definition found thereof, does not lead to conclusions regarding their definitive existence on the plasma membrane in-vivo as DRMs are obtained at 0-4°C far below temperatures associated with physiological conditions. In addition, solubilization of these “raft”-indicating fractions largely depends on the concentration of non-ionic detergent and has been indicated to rearrange the membranes by generating L_o phase spontaneously (Heerklotz, 2002). Later methods were employed to gain better insight into the plausible existence of rafts closer to physiological conditions which are

categorized as model membranes (biomimetic) and consist of Giant Unilamellar Vesicles (GUVs) and supported lipid bilayers (SLBs). Although evidence is present for the existence of rafts, the definition proposed at the Keystone Symposium is not comprehensive and leaves much to be understood. This general definition does not describe the transient nature of these "rafts" which has been indicated to have a range of duration of formation and subsequent dissipation (Subczynski & Kusumi, 2003) which is likely dependent upon a multitude of biological factors adding to their already complex nature. The size range and factors influencing the domain size has also been controversial (Prieto, et al., 2005). Nonetheless, these constituent determined ordered domains compartmentalize cellular processes in such a way that has functional consequences on proteins which prefer liquid-ordered regions as is evident for receptor-mediated signaling in mast cells (Young, Holowka, & Baird, 2003). Empirical evidence suggests that it is the coalescence of ordered regions of the plasma membrane which induces activation of transmembrane receptors (Sheets, et al. 2007). This coalescence is often induced by the cross-linking of proteins or lipids residing on the plasma membrane. Lipid rafts have been indicated in a variety of cellular processes, with T-cell activation being of pertinent regard in this thesis

BILAYER LATERAL HETEROGENEITY – PICKET FENCE MODEL

Of major influence on plasma membrane dynamics and a critical component of leaflet asymmetry is the presence of the cortical actin cytoskeleton. The actin cytoskeleton is a dynamic network of polymerized actin filaments and tubules which lies just beneath the inner leaflet of the lipid bilayer. It is now well established that the cytoskeleton can have a profound effect on the dynamics of membrane lateral heterogeneity and has be implicated in having an effect on rafts (Chichili & Rodgers, 2010). Therefore, the actin meshwork that lies beneath the cytosolic facing leaflet must be able to control the fluidity of the membrane to perturb purely spontaneous phase separation from being a solely dominating force at the plasma membrane. This model, named “anchored-protein picket fence”, was first introduced by Kusami and colleagues (Kusami et al., 2002). By observing a phospholipid, which is not considered part of raft portions, 1,2-dioleoyl-*sn*-glycero-3-phosphoethanolamine (DOPE) fluorescently tagged with Cy3 in its phosphate head group was found to be significantly altered by the actin cytoskeleton’s degree of polymerization in Large Unilamellar Vesicles (LUVs). No alteration of diffusion was found after reduction of the extracellular matrix (ECM) by treatment with trypsin nor could the reduction in diffusion be considered raft based as DOPE (1,2-dioleoyl-sn-glycero-3-phosphoethanolamine) has been implicated as an unsaturated lipid known to exist outside nor partition into L_o nanodomains. This rules out the effect of the ECM or rafts acting as barriers for diffusion in this model. After treatment with Latrunculin-A (Lat-A), confinement of DOPE was found to be less restricted during single particle tracking. Therefore, the “anchored-protein picket fence” model suggests that the actin meshwork as the cytosolic face of the plasma membrane is the heart of transient confinement of the reduction in diffusion rates found at the

plasma membrane. In this model, it has been implicated that transmembrane proteins act as binding sites, or “pickets” spanning across the bilayer, tethering the membrane to the actin cytoskeleton. The fraction of transmembrane proteins tethered to the action cytoskeleton are relatively immobile, which induces a local increase in viscosity of lipids and proteins. In addition, these immobile transmembrane proteins act as contact points, or kinetic barriers for proteins / lipids that diffuse directly into these protein fractions. Consequently, these “picket” transmembrane proteins exclude their immediate membrane areas by causing an increase in friction and remain as an immobile barrier of lateral diffusion. The “fence” portions of the model are the segmented regions of actin filaments spanning between points of tethered transmembrane proteins. These regions are not dependent on cholesterol content and therefore remain independent of the traditional effects of “raft”-like domains. Between tethered transmembrane proteins and cords of actin filaments, exists free or Brownian diffusion. In the case of a protein or lipid diffusing into actin filaments outlining these zones of free diffusion, they may or may not have enough kinetic energy to permit crossing into the next confinement zone. Diffusion past “fences” or actin meshwork requires “Hop” diffusion where it is thought that the actin filament is temporarily dissociated or the protein/lipid diffusing across the filamentous barrier possesses enough kinetic energy to overcome the active barrier. The “anchored protein picket-fence” model suggests that macroscopic diffusion will express an overall decrease in lateral diffusivity depending on the scale of observation. At large observation scales ($\geq$micrometer) the diffusion shows this general decreased diffusion due to filaments and immobile transmembrane proteins, but at the nanoscale, faster free-diffusion will be present.

BILAYER ASYMMETRY OF LIPIDS / STEROLS

It is clear that lateral inhomogeneity dictated by phase is distinguished by factors including temperature, and interactions between lipid / sterol constituents on the plasma membrane. In addition, it has been demonstrated that the cytoskeleton can play an active role in mediating protein / lipid diffusion on the plasma membrane. It is also important, in particular to the objectives of this thesis, to examine the asymmetry between opposing lipid monolayers in the lipid bilayer. The factors which distinguish the two leaflets include the relative abundance of certain types of lipids, the influence of the cortical actin cytoskeleton, and distribution of cholesterol between the two leaflets. These factors may have a profound impact on the phase behavior hypothesized to exist on the plasma membrane. Previous biochemical studies have shown there is a disparity between the types of lipids which reside on the inner and outer leaflet of eukaryotic plasma membranes. In general, PC and Sphingomyelin (SM) are predominantly found at the outer leaflet of the bilayer, while amine attached lipids such as phosphatidylethanolamine (PE), phosphatidylinositol (PI), and phosphatidylserine (PS) are mostly on the inner leaflet (Feigenson et al. 2008). The differences in the lipid constituents has obvious implications for variance in phase behavior between the two leaflets as the lipids named have, in general, a higher degree of polyunsaturated carbon tails which reduces packing efficiency. With potential difference in L_d phase between the inner and outer leaflets, it is important to gain a better understanding of where cholesterol resides between the two leaflets. Recent molecular dynamics simulations of the eukaryotic lipid bilayer yield insight into a moderately cholesterol enriched outer leaflet with cholesterol distributing asymmetrically (~54% and 46% cholesterol content on the outer and inner leaflet respectively (Ingólfsson, et al., 2014). This finding implies that the outer leaflet possibly contains an increase in L_o regions

compared to the inner leaflet although other hypotheses exist as to the exact partitioning of cholesterol between leaflets of the plasma membrane (Devaux & Morris, 2004).

This leads to the question of interleaflet coupling and registration between domains of the two lipid monolayers which makeup the plasma membrane. This question is critical to understanding cellular processes induced by transmembrane signaling proteins which are thought to partition into ordered or disordered regions depending on their chemical composition (hydrophobic / hydrophilic moieties). Whether or not these domains exist in registry in-vivo and to what extent is still not clear. Also, the way in which interleaflet coupling may exist is also unknown. Much of our understanding of this depends on molecular dynamic (MD) simulations and is rightfully understood through the lens of statistical mechanics.

There are a number of theories which are thought to contribute to interleaflet coupling which include interdigitation between acyl chains of opposing leaflets, interleaflet cholesterol translocation, and surface tension which may or may not be mutually exclusive (Collins, 2008). Noteworthy is the experimental and theoretical evidence which suggests that domains formed on one leaflet must span the entire bilayer. On the theoretical side, the bilayer mid-plane can be thought of as a two-dimensional interface between two liquid phases. These liquids are composed of carbons of varying chain length, each of which exhibit line tension with the opposing carbons which scale with interfacial area. Although the exact mechanism of coupling is not addressed, a free energy term in molecular simulations shows that when a coupling term is applied, domains on one leaflet prefer to match the domains in the opposing leaflet to reduce an incurring free energy penalty (Putzel & Schick, 2008). Interleaflet coupling has also been demonstrated experimentally in SLBs and unsupported bilayers (Naumann, 2007; Collins & Keller, 2008). In both studies, phase separation on one leaflet could impose phase separation

on the opposing leaflet in registration with each other although this is heavily influence by the phospholipid ratios constituting each monolayer.

Not yet addressed are the influences of membrane curvature on interleaflet coupling. It is intuitive that any perturbation to the interfacial line tension present at the bilayer mid-plane could have effects on domain registration and leaflet coupling. Neutron scattering experiments on unilamellar vesicles (ULVs) composed of ternary mixtures of DOPC (1,2-dioleoyl-sn-glycero-3-phosphocholine), DPPC (Dipalmitoylphosphatidylcholine), and cholesterol show an increase in curvature (decrease in mean vesicle radius) which results in an increase in the fraction of the bilayer composed of L_o domains (Katsaras et al., 2008). Curvature and domain registry taken together, can affect miscibility of bilayer constituents. There lies the possibility of affecting phase registration and therefore coupling between lipid monolayers in-vivo although no direct experimental evidence of this exists.

RBL-2H3 MAST CELL

A cellular model used for studying the plasma membrane is the rat basophilic leukemia (RBL) mast cell due to its antigen-induced / antibody-mediated signal transduction pathways. A particular example of this is multivalent antigen-mediated Immunoglobulin E (IgE) high affinity receptor complex FcεRI. As mast cells are part of the innate immune system, aggregation of IgE-FcεR1 complexes by multivalent antigen results in cellular degranulation releasing histamine among other physiologically active amines (Nilsson et al., 2001). FcεRI is a native transmembrane protein, and is composed of four subunits which are named α, β, and γ_2. The α subunit has both an intramembrane and extracellular portion. The extracellular portion of the α peptide has two immunoglobulin-like domains for high affinity binding to the Fc fragment of IgE in 1:1 stoichiometry and the extracellular portion of the α subunit is the only portion required for binding to IgE (Keown et al., 1995). The β subunit contains four transmembrane domains leading to the two γ polypeptides which form a homodimer linked by a disulfide bond which span the membrane and have regions both in the cytosolic and ECM (Kraft & Kinet, 2007). FcεRI is maintained as a tetrameric complex on the bilayer by noncovalent and hydrophobic interactions (Kinet, 1999). Since a large fraction of the FcεRI complex and the lipid-anchored proteins, which participate in initial phosphorylation events, interact with the hydrocarbon core of the lipid bilayer, it is necessary to investigate the plasma membrane of RBL mast cells to characterize the role of the surrounding lipid matrix on the receptor.

Previous studies indicate cross-linked IgE-FcεRI as well as inner-leaflet bound Lyn kinase as associating with ordered regions on the plasma membrane through a variety of

biochemical and biophysical techniques. Biochemical studies involving cholesterol depletion from RBL-mast cells using methyl-β-cyclodextrin (MβCD) have shown a loss of cross-linked IgE-FcεRI and Lyn kinase from DRMs under Triton X-100 solubility conditions while outer-leaflet GPI-anchored proteins, known to partition into ordered-like regions remained intact (Sheets, Holowka, & Baird, 1999). It has also been shown that the specific activity of Lyn kinase is higher for fractions derived from ordered-like regions (Young et al., 2003). These studies suggest that the phosphorylation events of Immunoreceptor Tyrosine-based Activation Motifs (ITAMs) after cross-linking by multivalent antigen could possibly be based on the way in which Src-family kinases such as Lyn are anchored to the inner-leaflet of the plasma membrane that allows partitioning into ordered-like regions could have a significant role in initial signaling events. In summary, inherent plasma membrane heterogeneity plays an important role in the initial events of mast cell signaling which is further supported by cutting-edge super-resolution microscopy investigations in our laboratory (Shelby et al., 2016).

Previous studies have shown that fluorescently tagged Lyn-kinase colocalizes with cross-linked IgE receptors (Holowka, Sheets, & Baird, 2000). The idea that the acyl chain anchoring of Lyn could influence co-redistribution with cross-linked receptors was investigated further using confocal imaging of live RBL-2H3 cells comparing three green fluorescent protein (GFP) constructs with differing acyl chain anchors (Pyenta, Holowka, & Baird, 2001). Two constructs were used:

- Lyn-EGFP is an endogenous Lyn analog bound to EGFP, PM-EGFP is a construct which contains the N-terminal sequence comprising 20 amino acids which code for the palmitoyl and myristoyl (PM) acylation sites which anchor it to

the inner-leaflet but does not contain its Src-homology 2 (SH2) or other protein binding domains

- EGFP-GG is a construct which has a C-terminal and polybasic sequence similar to K-ras, but with modification for geranylgeranylation (GG) as the acyl chain anchor to the inner-leaflet.

This previous study shows the colocalization of PM-EGFP with cross-linked IgE receptors using fluorescence confocal microscopy, while EGFP-GG shows weaker colocalization. The hypothesis that ordered-like regions of the plasma membrane are coalesced upon antigen stimulation and therefore functionally relevant to IgE receptor signal transduction is supported by the acyl chain anchor dependence of these named Green Fluorescent Protein (GFP) constructs.

Although these previous studies provide strong evidence for ordered regions of the plasma membrane playing a crucial role in antigen / antibody mediated signaling, the transient nature and size of these hypothesized domains makes them rather elusive to direct observation *in-vivo*. Equipped with the understanding that the plasma membrane exhibits lateral fluidity which differs between ordered and disordered regions, it is desirable to measure and quantify these diffusion processes occurring on the plasma membrane to gain insights into membrane proteins' spatiotemporal dependence on membrane fractions that exists in ordered or disordered states. In doing so, the nature of transient nanodomains can be unveiled in their relation to receptor mediated signaling and in turn will shed light on the biological relevance of these domains on cell signaling processes.

FLUORESCENCE CORRELATION SPECTROSCOPY

For the context of this study, the best-fit methodology for measuring plasma membrane dynamics in a non-invasive manner is Imaging Total Internal Reflection Fluorescence Correlation Spectroscopy (ITIR-FCS). To introduce FCS, let's first consider particles in solution which are in thermal equilibrium and expressing free diffusion (i.e. Brownian Motion). The particles will exhibit fluctuations in the distance traveled given a set time. If the particles are distinctly visible in the fixed volume we can certainly count them. If the particles are left unperturbed they will exhibit fluctuations which interrupt the local equilibrium which will be dissipated in a characteristic time. One can quantify these local fluctuations using autocorrelation functions. Therefore, FCS is a technique used to study the process of diffusion where the particles are visualized by their fluorescent properties. Fluorescence intensity of the particles from a small observation volume is monitored over time. The intensity trace is autocorrelated temporally to generate the autocorrelation function (ACF) which decays with time. The characteristic decay time of the ACF is called the diffusion time which is a measure of average time particles in solution take to travel across the observation volume. The diffusion time is inversely proportional to the lateral diffusion constant (D). The amplitude of the ACF at zero lag time is inversely proportional to the number of particles (N) within that observation area (i.e., steady state concentration).

The principle of the autocorrelation function (ACF or G(τ)) is the measure of self-similarity of an intensity trace (I(t)) between its beginning and subsequent time off-sets. The self-similarity is quantified by the relative overlap of area under the curve of the fluctuations from the average intensity trace in a given observation volume at its initial time and that of the intensity trace off-set by a subsequent time. Although the ACF function's full derivation is beyond the scope of this thesis, in order to provide a mathematic foundation for understanding, the following brief synopsis of the ACF function is provided.

The temporal fluctuations in intensity trace from the average renders the equation:

$$\delta I(t) = I(t) - \langle I(t) \rangle$$

The general form of G(τ) is given as the following:

$$G(\tau) = \frac{\langle I(t) I(t+\tau) \rangle}{\langle I(t) \rangle^2}$$

This general form of the ACF assumes stationarity of temporal fluorescence which can be shown mathematically as the following equation:

$$\langle I(t) \rangle^2 = \langle I(t) \rangle \langle I(t+\tau) \rangle^2 = \langle I(0) \rangle^2 \text{ where } t, \tau = 0$$

By making subsequent substitutions using the definition of temporal intensity fluctuations as well as making accurate assumptions, a more reduced form the general ACF formula can be obtained. Ignoring the normalizing denominator and substituting our definition of I(t) gives:

$$G(\tau) = \frac{\langle \big(\delta I(t) + I(t)\big)(\langle I(t+\tau) \rangle + \delta I(t+\tau)) \rangle}{\langle I(t) \rangle^2}$$

Expanding the numerator we find:

$$= \frac{\langle I(t)\rangle^2 + \langle \delta I(t)\delta I(t+\tau)\rangle + \langle I(t+\tau)\rangle\langle \delta I(t)\rangle + \langle I(t)\rangle\langle \delta I(t+\tau)\rangle}{\langle I(t)\rangle^2}$$

By recognizing the temporal fluorescence fluctuation does not change (stationarity) and by dividing the denominator into the numerator as indicated we find the following equation:

$$= 1 + \frac{\langle \delta I(\tau)\delta I(0)\rangle}{\langle I(t)\rangle^2}$$

Where $I(t)$ and $\delta I(\tau)$ can be written in the following way:

$$I(t) = \kappa \int_{-\infty}^{\infty} W(\vec{r})C(\vec{r},t)d\vec{r}$$

$$\delta I(\tau) = \kappa \int_{-\infty}^{\infty} W(\vec{r})\delta C(\vec{r},\tau)d\vec{r}$$

κ denotes brightness, $\vec{r}$ is the spatial coordinate, t is time, $C(\vec{r},t)$ is the concentration at spatial coordinate $\vec{r}$ and time t. $W(\vec{r})$ describes the observation volume and can be approximated as Gaussian and contains the product of the intensity profile of the focused excitation beam $I(\vec{r})$ and the fluorescence at position $\vec{r}$ after spatial limits being applied by the microscope pinhole.

$$W(\vec{r}) = I_0 e^{-\frac{2x^2}{\omega_0{}^2}} e^{-\frac{2y^2}{\omega_0{}^2}} e^{-\frac{2z^2}{\omega_z{}^2}}$$

Where the ω_o and ω_z represent the beam waist lengths in their respective axes as indicated by numerator variables, and I_0 is the maximum intensity at the focal point of the beam.

Substituting the Gaussian approximation expression for $W(\vec{r})$ into expressions for $I(\tau)$, one can represent average temporal fluorescence in the following way after integration over all coordinates:

$$\langle I(t)\rangle = \kappa\left(\frac{\pi}{2}\right)^{\frac{3}{2}} I_0 {\omega_0}^2 \omega_z \int_{-\infty}^{\infty} C(\vec{r},t)d\vec{r}$$

Substituting expressions found for $\langle I(t)\rangle$ and $\delta I(\tau)$ back into the general ACF one can simplify to render:

$$G(\tau) = \frac{1}{\langle C\rangle^2}\cdot\frac{8}{\left(\pi^{\frac{3}{2}}{\omega_0}^2\omega_z\right)^2}\int_{-\infty}^{\infty}\int_{-\infty}^{\infty} W(\vec{r})W(\vec{r}')\langle C(\vec{r},0)\delta C(\vec{r}',\tau)\rangle d\vec{r}d\vec{r}'$$

$$\langle C(\vec{r},0)\delta C(\vec{r}',\tau)\rangle = \langle C\rangle\cdot e^{-\frac{(\vec{r}-\vec{r}\prime)^2}{4\tau D}}\cdot 8^{-1}(\pi\tau D)^{-\frac{3}{2}}$$

Where the expression provided for $\langle C(\vec{r},0)\delta C(\vec{r}',\tau)\rangle$ can be derived from Fick's laws of diffusion, and D represents the diffusion constant.

After substitution of $\langle C(\vec{r},0)\delta C(\vec{r}',\tau)\rangle$ back into $G(\tau)$, and recognizing the definition of effective focal volume in confocal microscopy $\left(V_{eff} = \frac{(\int W(\vec{r})d\vec{r})^2}{\int W^2(\vec{r})d\vec{r}}\right)$ one can arrives at the ACF for a 3D system:

$$G(\tau) = 1 + \frac{1}{N}\left(1+\frac{4\tau D}{{\omega_0}^2}\right)^{-1}\left(1+\left(\frac{4\tau D}{{\omega_0}^2}\right)\left(\frac{\omega_0}{\omega_z}\right)^2\right)^{-\frac{1}{2}}$$

Equation 1. ACF for Confocal Microscopy

Where N represents the average number of particles within the observation volume and can be extracted from the amplitude of the autocorrelation function $G(0)$.

ILLUMINATION BY TOTAL INTERNAL REFLECTION

To illuminate molecules at the membrane and to improve signal to noise ratio (SNR), it is desirable to control the incidental light used to fluoresce molecules such that only fluorophores located at or near the membrane are excited. This can be achieved through total internal reflection fluorescence (TIRF) which produces an evanescent wave at the ventral membrane and in turn illuminates molecules located at the membrane surface.

When light travels from one medium to another, Snell's law states that the incidental light angle and the refractive index of the first medium the light passes through is proportional to the refractive index of the second medium and the angle of refraction. This is mathematically stated in Snell's Law of Refraction as $n_1 \sin\theta_1 = n_2 \sin\theta_2$ where $\theta_1$and θ_2 are the incidental and refractive angles of the light and n_1 and n_2 are the indices of refraction for first and second mediums respectively. $n_1 \sin\theta_1$ can also be referred to as the numerical aperture (NA) of the microscope objective that is used to focus the incident light at the sample. In order for the incidental light from an optically dense medium to reflect away from the boundary axis it has with a rarer medium, it must have an angle larger than what is known as the critical angle (θ_c). The critical angle can be found from Snell's Law of Refraction as

$$\theta_c = Arcsin\left(\frac{n_2}{n_1}\right)$$

Equation 2. Snell's Law of Refraction

Therefore, the angle of incidental monochromatic light used to excite fluorescent molecules located at the membrane must be greater than or equal to that of θ_c. The incidental light coming from an optically denser medium does not propagate through the rarer medium when the incident angle is greater than the critical angle. However, the electromagnetic field of light is not discontinuous at surface plane of the two medium and will produce a non-propagating evanescent wave in the rarer medium. The intensity of the evanescent wave, however, decays exponentially along the z-axis (parallel to the optical axis of incident light) of the two mediums (Breuer et al., 2008). This exponential decay along the z-axis is expressed using the following equation:

$$I(z) = I_o exp(-\frac{z}{d})$$

Equation 3. Exponential decay along the z-axis

Where the function I(z) is the intensity of the evanescent wave at a given z-axis position from rarer medium, I_o is the intensity of the evanescent

The distance of which the evanescent wave penetrates is found by the following expression:

$$d = \frac{\lambda_i}{4\pi n_1}(NA^2 - {n_2}^2)^{-\frac{1}{2}}, NA = \sin\theta_1 n_1$$

Equation 4. Distance of which the evanescent wave penetrates

Where λ_i is the wavelength of incidental monochromatic light used to excite fluorophores. The penetration depth along the z-axis of the evanescent wave field is particularly pliable to increase SNR and limit the depth to that of the width of the cell membrane. From the above equation, one can see that increasing the NA will reduce the penetration depth either by adjusting the angle of light from the denser medium or by increasing its index of refraction. Hence, mineral oil is used as the immersion medium of the objective in all experiments contained in this study for high refractive index (1.518).

The ACF derived above for confocal microscopy differs from that of the ACF fitting function used for TIRF microscopy in that $G(\tau)$ for the TIRF case is 2-D and involves determination of the effective area by convolution of microscope point spread function (PSF) with the size of CCD chip of the camera at the object plane, which has been recently developed. For the full derivation please see (Bag, 2014 & Sankaran 2012).

$$G(\tau) = \frac{1}{N}\left(\frac{\operatorname{erf}(p(\tau)) + \frac{\left(e^{-(p(\tau))^2} - 1\right)}{\sqrt{\pi}p(\tau)}}{\operatorname{erf}\left(\frac{a}{\omega_0}\right) + \frac{\omega_0}{a\sqrt{\pi}}\left(e^{-\frac{a^2}{{\omega_0}^2}} - 1\right)}\right)^2 + 1\,;\; p(\tau) = \frac{a}{\sqrt{4D\tau + {\omega_o}^2}}$$

Equation 5. ACF for TIRF Microscopy

In this expression, $\boldsymbol{\omega_o}$ represents the lateral portion of the observation volume (just as in equation 1), $\boldsymbol{\tau}$ is the lag time, $\boldsymbol{D}$ is the diffusion constant, and $\boldsymbol{a}$ represents the pixel side length.

FCS DIFFUSION LAW

In addition to fitting using the ACF, the FCS diffusion law is also an important tool for extracting data for FCS measurements to gain information regarding membrane heterogeneity below diffraction limit. It works to uncover this information based on principles of spot variation FCS. The FCS diffusion law provides a description of the dependence of time for a particle diffusing through an effective area (τ_D) on the effective area of the system (A). Rather than making multiple measurements at various sizes of effective areas as is found in spot variation FCS performed in other FCS modalities, Imaging FCS (IFCS) used in this study performs effective area changes to show τ_D dependence on effective area (A) post-acquisition of image file by binning the pixels intensity values. This removes the requirement of multiple measurements of variable spot sizes. In this thesis, pixel binning between 2x2-5x5 pixels are performed to achieve optimal statistics. After plotting multiple points of τ_D as a function of effective area (A), a linear fit on the data can be performed to acquire the value of the y-intercept, the τ_0 value. The τ_0 value reveals the dynamics observed on the membrane which are associated with various nanoscale structural determinants. For unhindered, Brownian diffusion, this linear equation should render a τ_0 value of 0 as D is space-invariant. In the case of anomalous diffusion caused by nanodomains or cytoskeletal interference, D will vary as the effective area increases such that τ_0 values will be positive or negative (“hop” diffusion), respectively (Wawrezinieck et al., 2005).

The mathematical expression for the diffusion law of FCS measurements is:

$$\tau_D(A) = \frac{A}{4D} + \tau_0$$

Equation 6. Diffusion Law for FCS measurements

Here, the τ_D are the experimentally determined times of diffusion at an effective area A. τ_0 is the extrapolated time of diffusion at A = 0 using Weighted Least Squares (WLS) regression. The effective area, A, in the case of IFCS, is a result of the convolution of the point spread function (PSF) with the pixel area (pixel side length squared) at the object plane which details the actual area of the membrane being observed.

Please see the Materials and Methods section on page 30 regarding how D and τ_D parameters are obtained from experiments conducted in this study.

THE PRESENT STUDY

With the evidence from previous experiments that the IgE receptor likely exists in an order-preferring lipid environment on the plasma membrane, it is necessary to further investigate the plasma membrane's effect on the IgE signaling pathway (Holowka et al., 2005). Evidence of the IgE receptors signaling dependence relying on the coalescence of ordered regions on the plasma membrane can be acquired by inducing disorder in an otherwise ordered domain and examining the biological effects of this change. Imaging FCS provides the means to observe the effect caused by obstacles for various fluorescently tagged proteins which exist in more or less ordered-like environments on each leaflet of the membrane. As previously indicated, these obstacles may be ordered-like nanodomains, but also may be

caused by actin filaments, both expected to induce a general decrease in diffusion constant (D) and increase in transient confinement (τ_0) of the proteins being observed.

The present study compares plasma membrane anchored proteins two of which (YFP-gl-GPI and PM-EGFP) are thought to partition into L_o-like domains and one believed to partition into less ordered regions, EGFP-GG, (L_d preferring) located on the outer and inner leaflet of RBL-2H3 mast cells under a variety of membrane constituent perturbing pharmacological conditions (Veatch et al., 2017; Baumgart et al., 2007; Simons et al., 2010). Each treatment condition is made in an attempt to disorder the otherwise ordered regions of the RBL plasma membrane and to observe the effects these treatments have on each leaflet of the bilayer. The pharmacological perturbations made to cultured RBL-2H3 cells include removal of cholesterol by use of methyl-β-cyclodextrin and integration short chain ceramides (C2- and C6- ceramide) or 7-ketocholesterol in the membrane. These conditions will be discussed in detail in the upcoming results and discussion chapters.

MATERIALS AND METHODS

Cell Culture. RBL-2H3 cells were maintained in monolayer culture as previously described (Pierini et al., 1996), and harvested using trypsin-EDTA (Life Technologies, Rockville, MD) 3-4 days after passage. Cells were cultivated in DMEM (Dulbecco's Modified Eagle Medium; Invitrogen) supplemented with 20% FBS (fetal bovine serum) and 1% streptomycin at 37°C in 5% (v/v) CO_2 humidified environment.

Sample Preparation and Transfection. Plasmid constructs including YFP-gl-GPI, palmitate and myristate-EGFP, and EGFP-geranyl geranyl were prepared previously as

described (Pyenta et al., 2001). Cultivated RBL-2H3 cells were seeded into glass covered dishes (35 mm Petri dish, 14 mm Microwell, No. 1.0 cover glass (0.13–0.16 mm), MatTek Corporation, Ashland, MA) containing 2 ml cell Dulbecco's Modified Eagle Medium (DMEM) + 20% FBS and incubated overnight. Stocks of anti-DNP (anti-2,4-dinitrophenyl) IgE labeled with Alexa-488 and unlabeled, were prepared as described (Subramanian et al., 1996). For labeling of FcεRI, labeled and unlabeled IgE was diluted in 1 ml Tyrodes buffer (4 M NaCl / 1M KCl / 0.5M $MgCl_2$ / 0.5M $CaCl_2$ / 1M Glucose / 1M HEPES in ddH_2O, pH 7.4) at 2 µg / ml of a 1:3 molar ratio (labeled and unlabeled respectively) and incubated with cells for 40 min. at room temperature (~22°C) then washed twice with 2 ml Tyrodes buffer prior to treatment In the case that transfection was required, cells were transfected in their respective glass covered MatTek dishes using 0.25 µg / µl plasmid, the appropriate amounts of FuGENE HD Transfection Reagent (Promega Corporation, Madison, WI) (6 µg / µl plasmid) and 100 µl Opti-MEM (ThermoFisher Scientific, US) per glass covered dish being used. After incubation with transfection reagents, cells were washed with 1 ml cell culture medium and then incubated in 2 ml cell culture medium 12-24 hours prior to imaging. Immediately prior to imaging, cell culture medium was discarded, washed twice with 2 ml Tyrodes buffer and replaced with 2 ml Tyrodes buffer. Pharmacological treatments by incubation subsequently described were performed in 1 ml Tyrodes prior to wash and replacing 2 ml Tyrodes buffer before imaging.

Methyl-β-Cyclodextrin Treatment. Cell culture tested, methyl-β-cyclodextrin (MβCD) was purchased from Sigma-Aldrich (US, Lot# 59H1082). A 20 mM MβCD stock solution was made in Tyrodes buffer and frozen between uses (-20°C). Reduction in concentration of MβCD was achieved by serial dilution prior to treatment in Tyrodes buffer shortly before conducting the measurements.

C2- & C6-Ceramide Treatments. C2- and C6-ceramide stock solutions were prepared at 22.5 mM and 5.5 mM in ethanol and DMSO solvent respectively. Prior to treatment, a small glass vial was prefilled with 1 ml Tyrodes buffer solution containing 1 mg / ml bovine serum albumin (BSA) prior to aliquots of ceramide being added for the desired concentration for cell exposure. After subtle mixing, the 1 ml Tyrodes + ceramide was added to MatTek dish pre-seeded with cells and containing 2 ml Tyrodes + BSA. It was then incubated at room temperature for 10 minutes prior to subsequent imaging. Imaging sessions for a single treatment typically extended for ~1 hr.

7-Ketocholesterol / MβCD Complex Preparation and Treatment.

7-Ketocholesterol (7-KC) was purchased from Sigma-Aldrich (US). 5% (w/w) MβCD stock solution was prepared by dissolving 250 mg of MβCD in 5 ml ddH_2O. Next, 1 ml of 15 mg / ml 7-KC was prepared in a glass vial. 400 µl of stock MβCD was added to a high-performance liquid chromatography (HPLC) vial on a hotplate at 80°C with occasional mixing. 4 x 10 µl aliquots of 7-KC/ethanol solution was added drop-wise to the HPLC vial allowing for 5-10 minutes to pass with occasional mixing. After the final (fourth) aliquot of 7-KC/ethanol solution, the HPLC vial was left on the 80°C hotplate for one hour without covering the vial to evaporate the majority of ethanol solvent. After one hour, the HPLC vial was covered, and stored at 4°C. Cells were treated with 15 µl 7-KC:MβCD complex diluted in 1 ml Tyrodes buffer solution at room temperature and incubated for 30 minutes at 37°C prior to imaging.

Cytochalasin D Treatment. Cytochalasin D (Aldrich Chem. Co., Milwaukee, WI) was kept at a stock solution of 1.95 µg / ml in DMSO. Cytochalasin D stock solution was subsequently diluted ~1:1000 in order to reach a concentration of 2 µM in Tyrodes buffer

solution. 1 ml of 2 μM Cytochalasin D solution was then aliquoted into MatTek dishes pre-seeded with RBL-2H3 cells and incubated at 37°C for 5 minutes prior to imaging at room temperature (~22°C).

Imaging Fluorescence Correlation Spectroscopy. Imaging of all samples was carried out at room temperature (~22°C) using a Leica DMIRB Inverted Confocal Microscope and a high NA oil immersion objective (100x, NA 1.47). For illumination of endogenous or synthetic fluorescently labeled proteins, a 488 nm Coherent Sapphire (Santa Clara, CA) laser was used. The laser beam was directed into the microscope by a combination of tilting angle mirrors after its intensity was attenuated by a neutral density filter to achieve optimal signal to noise ratio with minimal photobleaching. The incidental laser beam was then focused onto the back focal plane of the objective after reflection by a dichroic mirror. The objective immersion oil used was Olympus Type-F (refractive index of 1.518). Total Internal Reflection (TIR) was acquired via the last tilting mirror prior to the laser being directed into the microscope that of which the position could be changed steadily. The microscope was connected to an Andor iXon+ fast electron multiplying charge coupled device (EMCCD) camera through a side port. Image acquisition was done through Andor SOLIS software using an exposure time of 3.0 ms and kinetic series length of 80,000 frames. Regions of interest (ROIs) were specified generally in the middle of each cell measured, with a given pixel range usually at 40x40. Data were stored as 16-bit .TIFF files.

Under the circumstance of defocusing during measurements, the protocol was altered in order to circumvent this problem in the following way: the kinetic series length was lowered to 20,000 frames and performed four times while holding the same ROI size and position

provided by the Andor SOLIS software. These 20,000 frame image stacks were then concatenated through ImageJ software to compose a single 80,000 image stack.

FCS Data Analysis. Image series were saved as black and white 16-bit .TIFF files and intensity values for each pixel underwent temporal correlation using ImageJ plugin "ImFCS" software (available at http:// staff.science.nus.edu.sg/~chmwt/ImFCS.html) in order to obtain the autocorrelation functions (ACFs) of each pixel / binning within the ROI specified. Using the acquired ACF data, the "ImFCS" plugin fits the data using non-linear least squares regression for best fit of Equation 5 (ACF for TIRF Microscopy). All parameters are provided by the user for the fitting equation (except those which remain as fit parameters including N and D). After best fitting of the ACF data using equation 5 within the "ImFCS" software, the diffusion constants obtained are directly extracted. The FCS Diffusion Law provided in equation 6 is performed in the following manner within the "ImFCS" software: the pixelwise diffusion constants are obtained for various effective areas by binning of pixel intensities after which the diffusion constants are averaged. Once the average diffusion constant is obtained for the specified ROI, it is used as a constant in the diffusion law plot. In this case, the time of diffusion, τ_D, in equation 6 is not directly extracted from the ACF, but is provided by recognizing that $\frac{4D}{A} = \tau_D$ when $\tau_0 = 0$ (i.e. free diffusion) where D is the obtained average and A is the effective area obtained depending on pixel side length. Pixels were defined using a 2-5 binning scheme as this was found to be an optimal approach. A 2x2-5x5 binning was used for ROIs spanning 7x7 individual pixels (1x1) using default overlapping mode for improved statistics (Bag et al., 2016). In this manner, the diffusion law analysis is conducted by plotting data points of calculated τ_D as a function of effective area (A) and using weighted least squares regression to obtain the τ_D intercept (τ_0). Batch fitting of data from the exported Excel sheet by 'ImFCS' was done using

home-built code written in MatLab for multiple weighted least squares regression (WLS) where weights were approximated using the Standard Error of the Mean (SEM). See Appendix A.

Statistical Analysis. Statistical analysis was performed using Matlab's Statistics and Machine Learning Software package (MathWorks Natick, MA). After determination of non-normality by a quantile/quantile plot of the data, a Mann-Whitney U test was implemented to estimate the statistical significance of results compared to control.

RESULTS

For the purpose of identifying pharmacological conditions which have the ability to disrupt cholesterol-dependent liquid-ordered regions on the resting RBL-2H3 cell membrane, the transient confinement time (τ_0) and diffusion constants (D) exhibited by various membrane-bound proteins were measured using imaging total internal reflection fluorescence correlation spectroscopy (ITIR-FCS). The following results section includes three types of graphical representations of data collected in this study:

1) Average D and τ_0 values (y-axes) obtained per cell (colored box markers) as well the total average for all trials (black empty square marker) of a particular protein and treatment as indicated by the x-axis (e.g. Figure 1). Error bars denote the standard error of the mean (SEM). Total averages for all trials (9-10 cells) per protein / treatment ± standard deviation (SD) are provided in each table (e.g. Table 1).
2) Histograms of D and τ_0 values represent the combined distribution of D and τ_0 from all trials of a given fluorescent reporter and treatment condition (e.g. Figure 3). As indicated by their headers, histograms and their corresponding horizontal bar graph sets (below each histogram) are separated by the fluorescent reporter they represent and the

treatment series performed. These histograms are normalized by area for their direct comparison to other treatments also represented on the same axes.

3) Horizontal bar graphs, located below each histogram, are another way of direct comparison of the data presented in each histogram compared to their respective control distributions. Each horizontal bar graph is representation of the fraction of data points collected which exhibit either D or τ_0 values above or below ± 1 SD of the control distribution, and, in the case of τ_0, also the fraction of data points which hold a value below 0. The fraction of data points which are values greater than +1 SD from the mean of the control data set are represented by red color bars, and are regarded as the fraction of molecules contributing to "fast" diffusion in the case of D and "long" transient confinement time in the case of τ_0. Likewise, the gray bars represent the fraction of data points which are values below -1 SD from the mean of the control distribution and are regarded as "slow" diffusion or "short" transient confinement time. Yellow bars represent the fraction of data points contributing to the bulk of the data. As explained on page 24, green represents the fraction of molecules expressing "hop" diffusion which encompasses the fraction of data points holding τ_0 values below 0. Each horizontal bar set is representative of the histograms it is located under.

Effects of Short-Chain Ceramides on L_o Fluorescent Reporters

In order to reveal the effects on translational mobility by short-chain ceramides (C2- and C6-ceramide) on ordered regions of the lipid bilayer of RBL-2H3 cells, τ_0 and D values were obtained for RBL-2H3 cells transfected with outer-leaflet ordered region preferring protein YFP-GPI and inner-leaflet ordered region preferring PM-EGFP. Data collected for average τ_0 and D values per cell under these conditions are plotted for visualization of significant changes induced by treatment with ceramide compared to the control population in Figures 1 & 2. A significant increase in translational diffusion for YFP-GPI was found for treatment with 16 μM C6-ceramide (~ +33%) corresponding with a decrease in τ_0 (~16%) indicating increased fluidity and decreased lipid order caused by C6-Ceramide integration at outer-leaflet L_o-like regions under these conditions. However, incubation with 32 μM C2-ceramide resulted in significant decrease in τ_0 without significantly effecting the average D for YFP-GPI. These results are consistent with previous findings using FRET (Förster Resonance Energy Transfer) and fluorescence anisotropy where it was observed that C6-ceramide is more potent on a mole-per-mole basis than C2-ceramide at disordering cholesterol-dependent ordered regions of the lipid bilayer on RBL-2H3 cells (Gidwani et al., 2003). The effects of C2- and C6-ceramide at inner-leaflet ordered regions by PM-EGFP were also observed for comparison. Treatment with 32 μM C2-Ceramide showed no statistically significant change in average D of PM-EGFP just as in the case of YFP-GPI, but additionally showed no change in average τ_0. This result is rather surprising considering that there exists a high probability of short-chain ceramide translocation across the lipid bilayer after integration in the plasma membrane (Bai & Pagano, 1997). In order to extract information regarding subtle changes which may be less discernable when comparing the obtained averages of D and τ_0 in these cases, distributions of these data

are presented in Figures 3, 4, 5 and 6. The distribution of D for PM-EGFP broadens as a result of C2-ceramide treatment (Figure 5) expressing an increase in the variability for diffusion under this condition. In the case of C6-ceramide treatment, the τ_0 distribution does not change for PM-EGFP. YFP-GPI shows ~10% reduction in molecules exhibiting long transient confinement time (>+1 Standard Deviation) which corresponds with the 16% decrease in average τ_0 as mentioned. Interestingly, both YFP-GPI and PM-EGFP show an increase in their fractions of fast moving particles (~15 and 20% respectively) (Figures 3 & 5), but only YFP-GPI shows a corresponding increase in short transient confinement time (<-1 Standard Deviation) (Figure 4, gray bar).

To further investigate the fluidizing effect of C6-ceramide on L_o-like regions, the diffusion properties of Alexa488-IgE-FcεRI were observed by incubation with Alexa-488 labeled anti-DNP IgE prior to treatment with 16 μM C6-ceramide as described in Materials and Methods. C6-ceramide had no effect on the diffusion of Alexa488-IgE-FcεRI despite the symmetric increase observed for YFP-GPI and PM-EGFP (Figure 7). As shown in Figure 8, the distribution of τ_0 for Alexa-488-IgE-FcεRI under C6-ceramide treatment shows a shift consistent with the ~10% decrease in average value. Average values from all experiments performed using short-chain ceramides are summarized in Table 1.

Protein	Treatment	Diffusion Constant (μm^2/ s)	$\tau 0$ (s)	# of Cells	# of Samples
YFP-GPI	Control	0.33 ± 0.16	0.92 ± 0.35	9	2
	C2-Cer	0.34 ± 0.19	0.78 ± 0.30	10	2
	C6-Cer	0.44 ± 0.22	0.77 ± 0.30	10	2
PM-EGFP	Control	0.50 ± 0.18	0.44 ± 0.28	9	2
	C2-Cer	0.50 ± 0.24	0.42 ± 0.24	10	2
	C6-Cer	0.60 ± 0.21	0.40 ± 0.24	10	2
Alexa488-IgE-FcεRI	Control	0.23 ± 0.15	1.20 ± 0.83	10	2
	C6-Cer	0.23 ± 0.16	1.06 ± 0.73	10	2

Table 1. Summary of average results obtained from imaging FCS measurements on resting RBL-2H3 cells incubated with 32 μM C2- and 16 μM C6-ceramide in Tyrodes buffer solution (± SD)

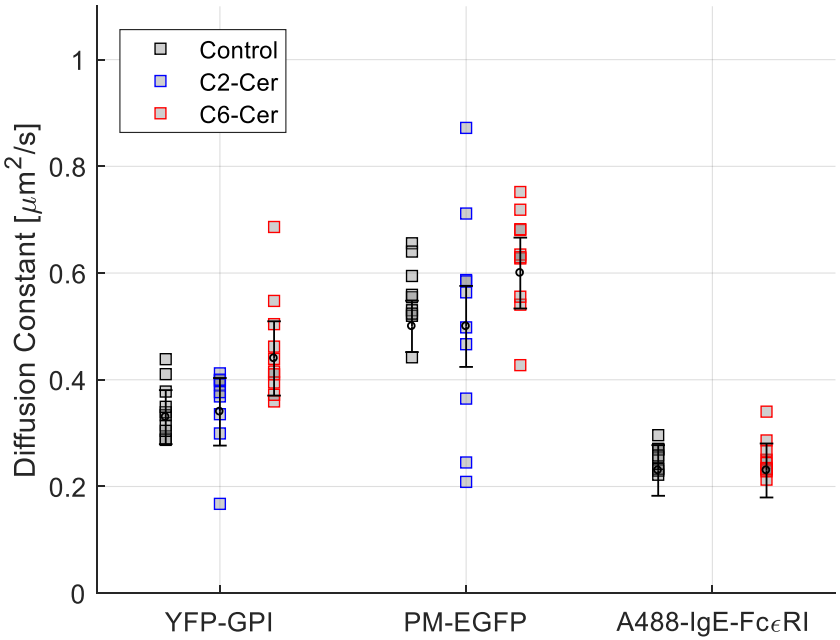

Figure 1. Effects of C2- & C6-ceramide on average D

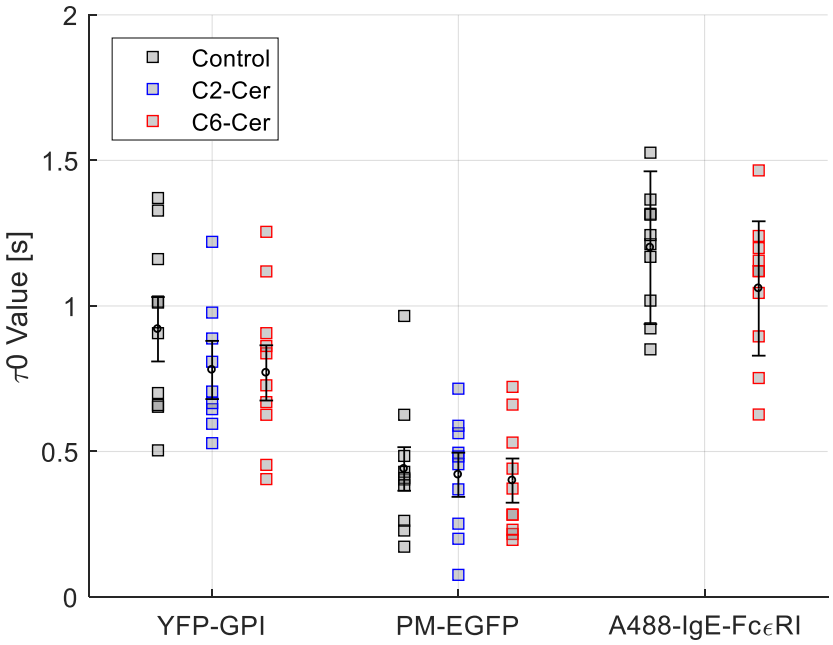

Figure 2. Effects of C2- & C6-ceramide on average τ_0

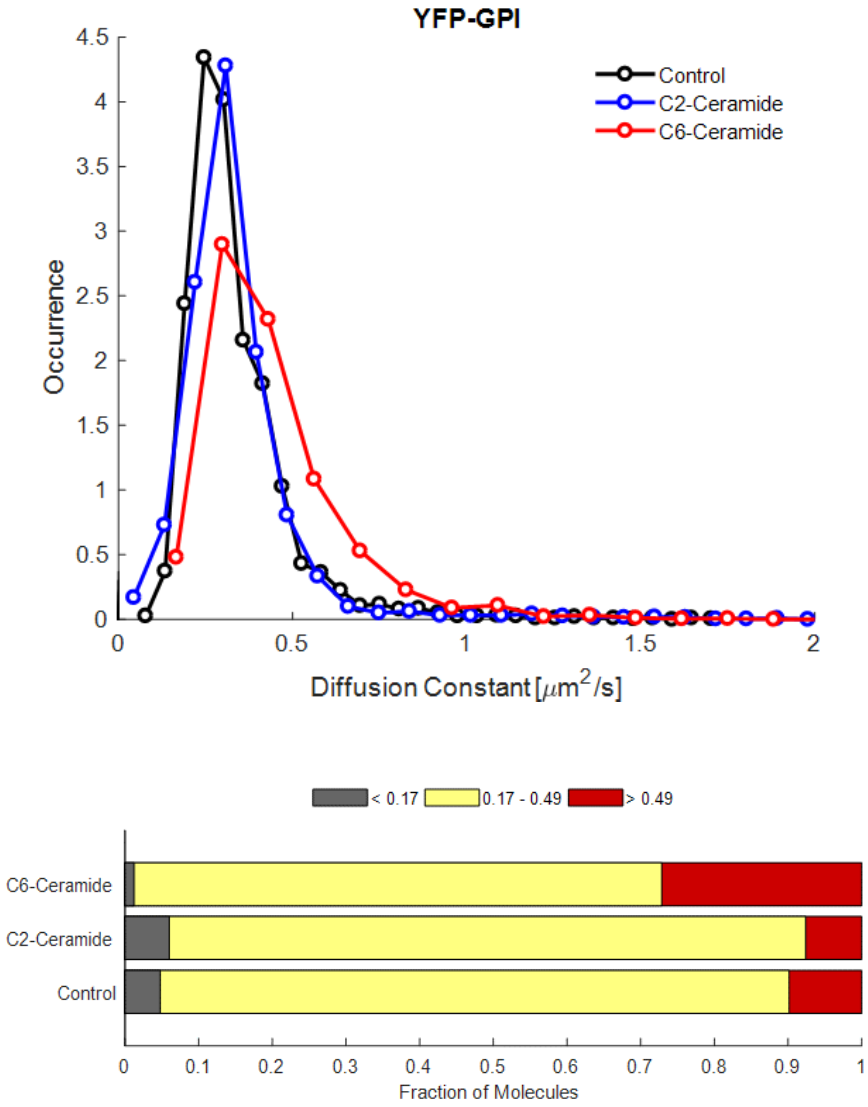

Figure 3. Effects of C2- & C6-ceramide on YFP-GPI D Distributions

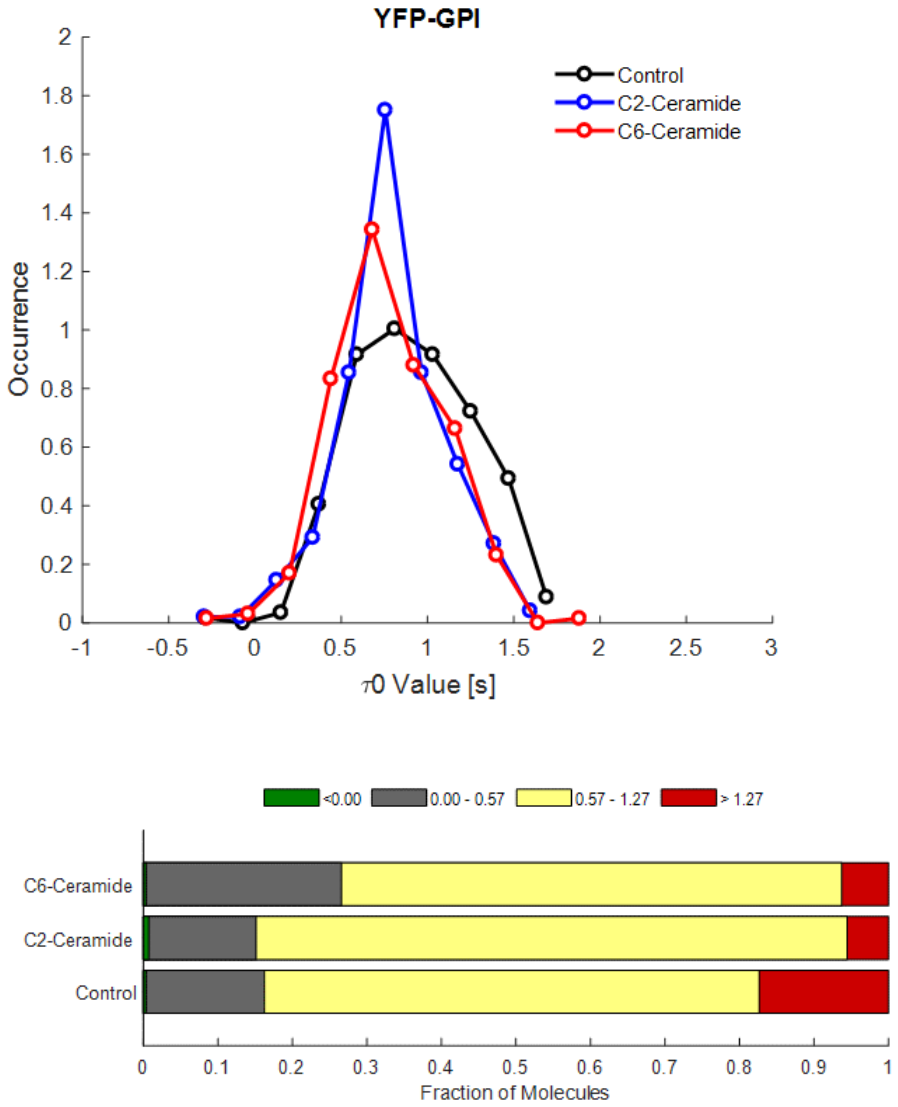

Figure 4. Effects of C2- & C6-ceramide on YFP-GPI τ_0 Distributions

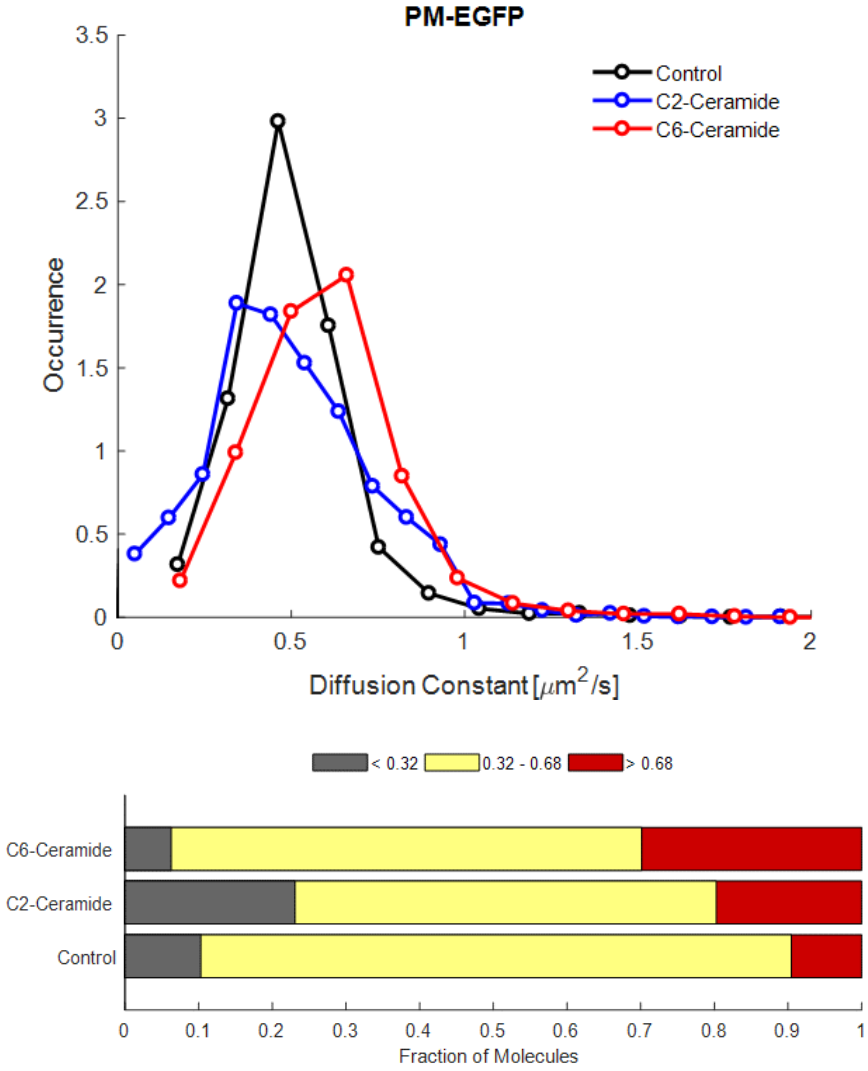

Figure 5. Effects of C2- & C6-ceramide on PM-EGFP D Distributions

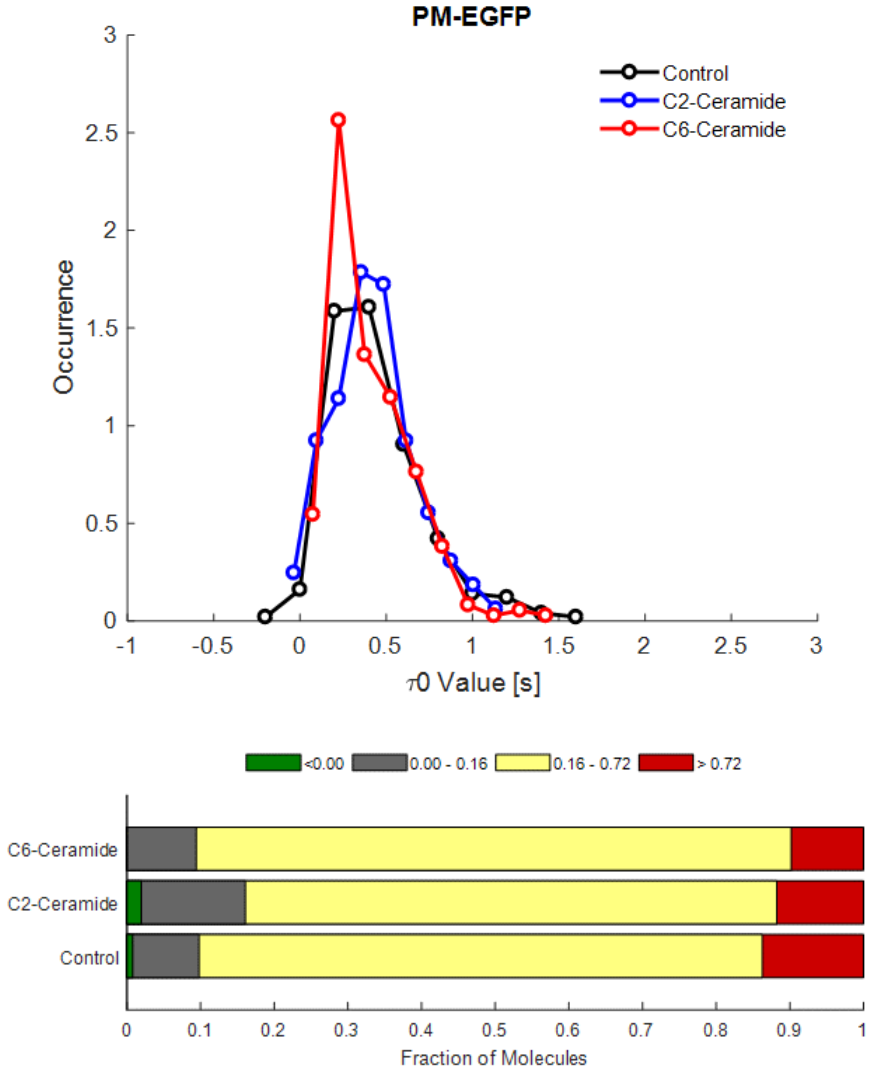

Figure 6. Effects of C2- & C6-ceramide on PM-EGFP τ_0 Distributions

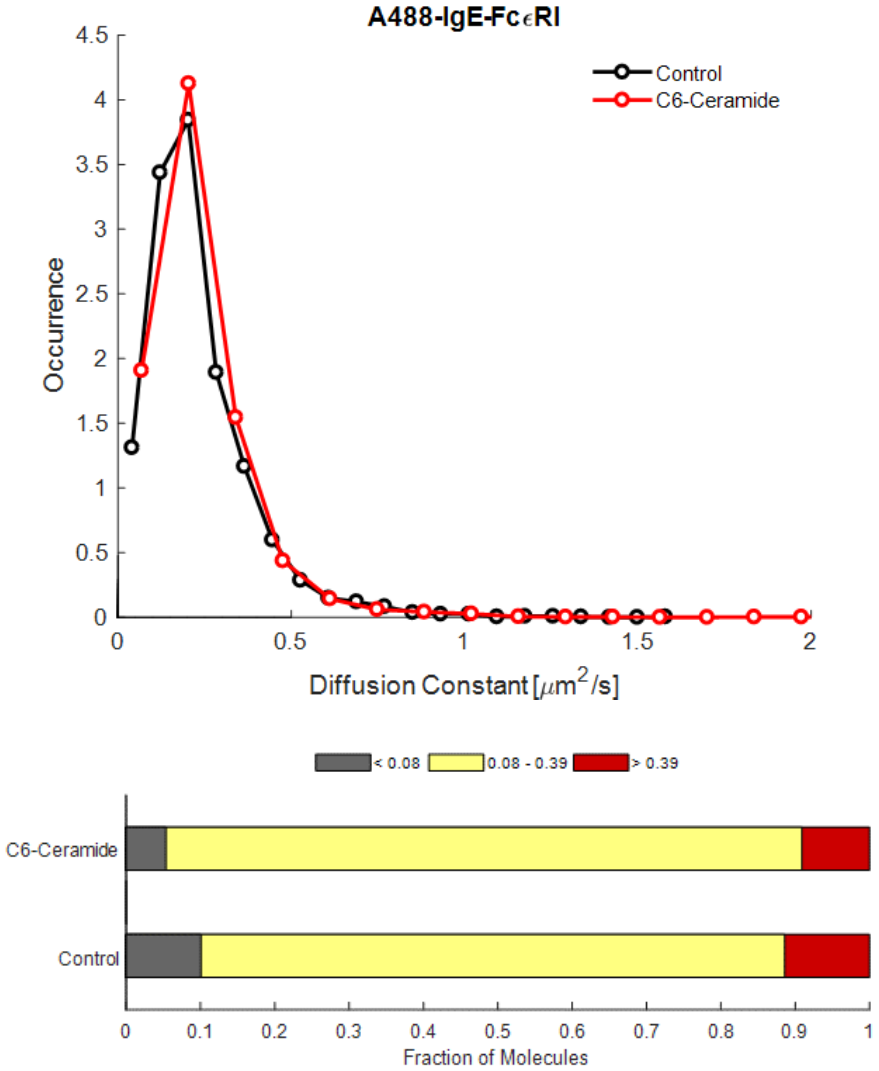

Figure 7. Effects of C6-ceramide on Alexa488-IgE-FcεRI D Distributions

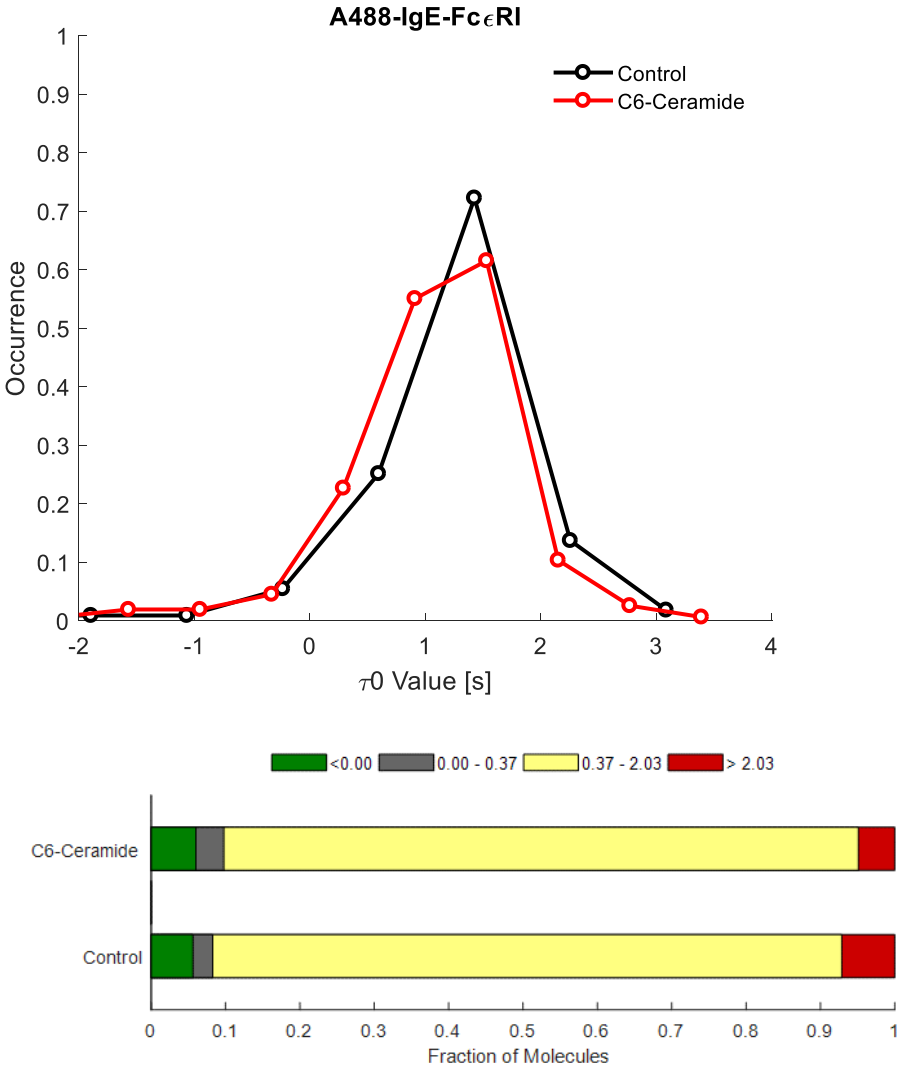

Figure 8. Effects of C6-ceramide on Alexa488-IgE-FcεRI τ_0 Distributions

Effects of Cholesterol Depletion on Inner and Outer Leaflet Lo / Ld Fluorescent Reporters

For the purpose of examining the relative effect of cholesterol depletion between monolayers, MβCD was incubated with resting RBL-2H3 cells for 30 minutes at 37°C 12-24 hours after transfection with either YFP-GPI or PM-EGFP plasmid constructs as described in Materials and Methods. Cholesterol removal by incubation with MβCD resulted in a significant decrease in average D and increase in τ_0 values for both YFP-GPI and PM-EGFP, but not for EGFP-GG (Figure 9, blue markers and Table 2). This decrease in lateral mobility exhibited by YFP-GPI and PM-EGFP and lack-thereof for EGFP-GG in a cholesterol depleted lipid environment is consistent with previous findings in this laboratory, namely that cholesterol depletion under these conditions causes the formation of ventral plaques (observed very close to bottom surface of the cell) containing L_o preferring proteins such as YFP-GPI and PM-EGFP, but not L_d preferring proteins such as EGFP-GG, and that these plaques exhibit a significant reduction or complete loss of lateral mobility as measured by Fluorescence Recovery After Photobleaching (FRAP) experiments (D. Holowka, unpublished observations). However, the relative changes in values obtained by FCS measurements indicate asymmetry between ordered regions on the outer and inner leaflets. While the D and τ_0 values for both reporters decrease and increase respectively, there is a stark contrast in the magnitude of change (Table 2) where lateral mobility is more restricted for YFP-GPI than for PM-EGFP. By looking at the normalized distributions of these data (Figures 11, 12, 13 & 14), it is apparent that the decrease in average diffusion is caused by an increase in the fraction of molecules presenting slow (< -1 SD from the mean) diffusion and long confinement time (> +1 SD from the mean). Notable is the lack of any change in average D by EGFP-GG (Figure 9) which is consistent with their lack

of partitioning into ventral plaques formed after cholesterol depletion (D. Holowka, unpublished observations). While the average D does not change in a cholesterol depleted environment, the distribution (Figure 15) for D values is broadened. Additionally, the distribution of τ0 values (Figure 16) shows an increase in average contributed by an increase in fraction of EGFP-GG molecules with longer transient confinement times (see discussion).

Effects of 7-Ketocholesterol on Inner and Outer Leaflet Lo / Ld Fluorescent Reporters

In the continued search for a suitable pharmacological treatment which would adequately disrupt cholesterol-dependent ordered regions on the RBL-2H3 cell plasma membrane, MβCD, preloaded with 7-ketocholesterol (7-KC) (1:1 molar ratio), was incubated with RBL-2H3 cells to incorporate 7-KC in the lipid bilayer. Such treatment is known to laterally disorder plasma membranes in Jurkat T cells. The addition of 7-KC on the RBL-2H3 plasma membrane however showed no significant change in average D obtained for YFP-GPI (outer-leaflet), but did induce an increase in average τ_0 (Figures 9 & 10). The normalized distribution of D values also shows no change from that of the control (Figure 11, red line), while that of τ_0 values indicates an increase in the fraction of YFP-GPI molecules exhibiting longer confinement times and a reduction in short confinement times (Figure 12). These observations are disparate with those found for inner-leaflet markers PM-EGFP and EGFP-GG. There is a significant uniform decrease in average D (~15%) for both PM-EGFP and EGFP-GG induced by 7-KC addition (Figure 9 & 10). Although the average τ_0 values increase for both of these reporters, the extent

of which varies between the two with PM-EGFP increasing by ~64% and EGFP-GG nearly doubling (Table 2). The normalized τ_0 distributions for these proteins show increased long transient confinement time (Figures 14 & 16), although perhaps to a lesser extent for PM-EGFP (red bars). A combination of treatments were performed in succession, first adding MβCD for cholesterol depletion and then addition of 7-KC as described in materials and methods (see discussion). D and τ_0 values were restored to closer to control levels in the case of YFP-GPI compared to that of only treatment with MβCD and reach an intermediate in long transient confinement between 7-KC and MβCD treatments alone (Figures 9 & 10, blue compared to green markers for YFP-GPI). This same set of succession of treatments had a different effect on PM-EGFP, where fraction of slow diffusing and long-transient confinement of PM-EGFP molecules was increased further than either 7-KC or MβCD treatments alone, which was not the case for EGFP-GG (Figures 14 & 16)

Protein	Treatment	Diffusion Constant (μm^2/ s)	τ0 (s)	# of Cells	# of Samples
YFP-GPI	Control	0.35 ± 0.20	0.83 ± 0.29	10	2
	MβCD	0.27 ± 0.19	1.55 ± 0.47	9	2
	7-KC	0.34 ± 0.14	0.95 ± 0.24	10	2
	MβCD + 7-KC	0.33 ± 0.17	1.16 ± 0.29	10	2
PM-EGFP	Control	0.56 ± 0.16	0.39 ± 0.19	10	2
	MβCD	0.51 ± 0.28	0.55 ± 0.26	10	2
	7-KC	0.47 ± 0.18	0.64 ± 0.28	10	2
	MβCD + 7-KC	0.44 ± 0.19	0.69 ± 0.22	10	2
EGFP-GG	Control	0.53 ± 0.16	0.42 ± 0.25	9	2
	MβCD	0.53 ± 0.28	0.53 ± 0.25	9	2
	7-KC	0.45 ± 0.20	0.81 ± 0.34	9	2
	MβCD + 7-KC	0.45 ± 0.19	0.74 ± 0.27	9	2

Table 2. Summary of average results obtained from imaging FCS measurements on resting RBL-2H3 cells incubated with MβCD, 7-KC, or MβCD then 7-KC in Tyrodes buffer solution (± SD).

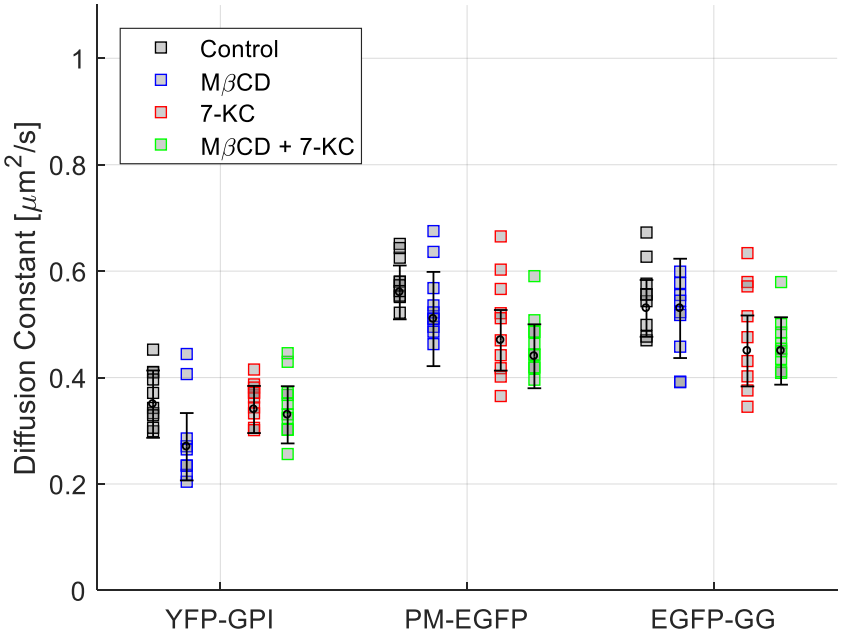

Figure 9. Effects of Cholesterol Depletion & 7-KC Addition on D Averages

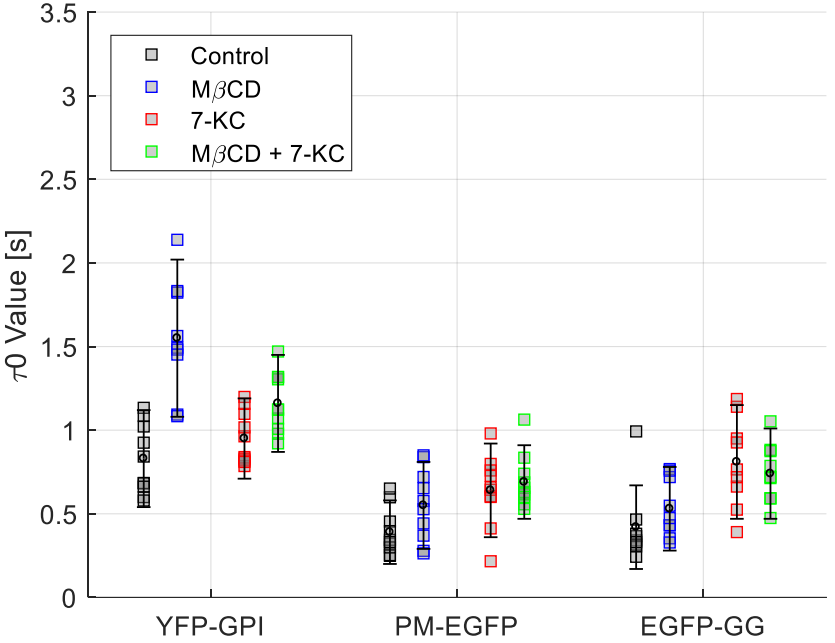

Figure 10. Effects of Cholesterol Depletion & 7-KC Addition on τ_0 Averages

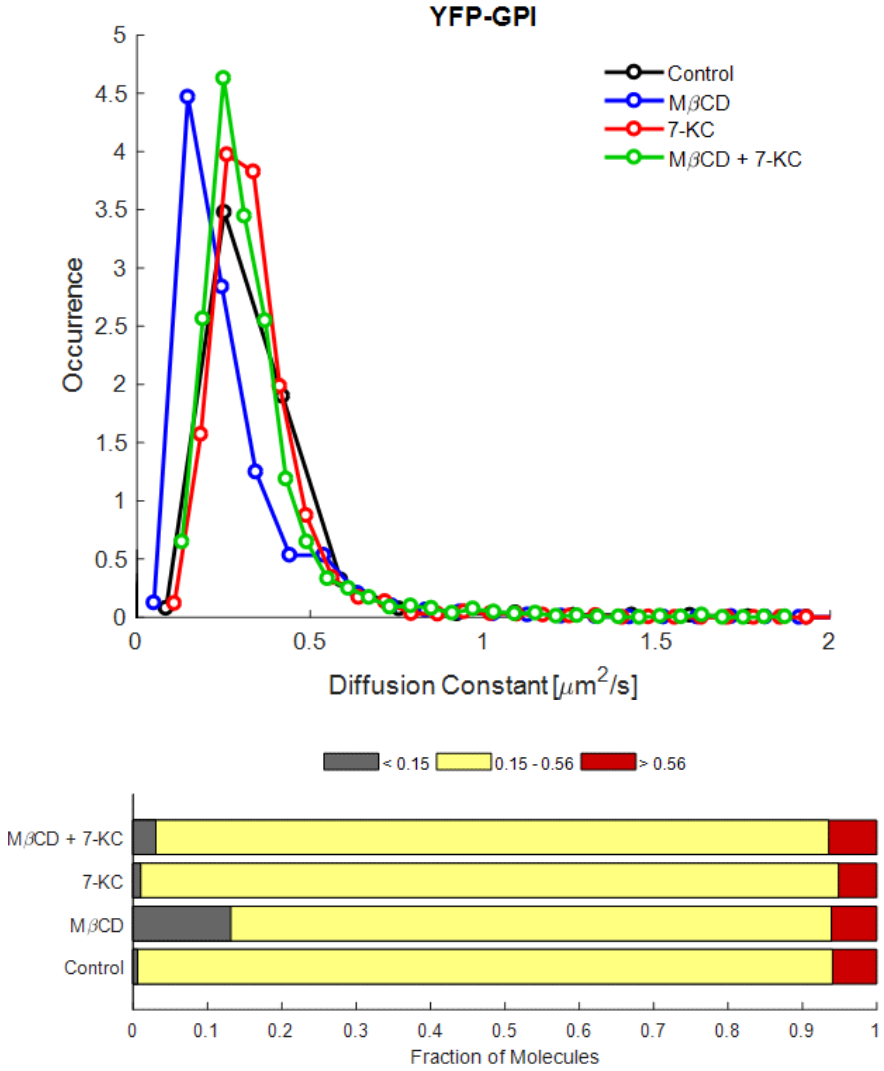

Figure 11. Effects of Cholesterol Depletion & 7-KC Addition on YFP-GPI D Distributions

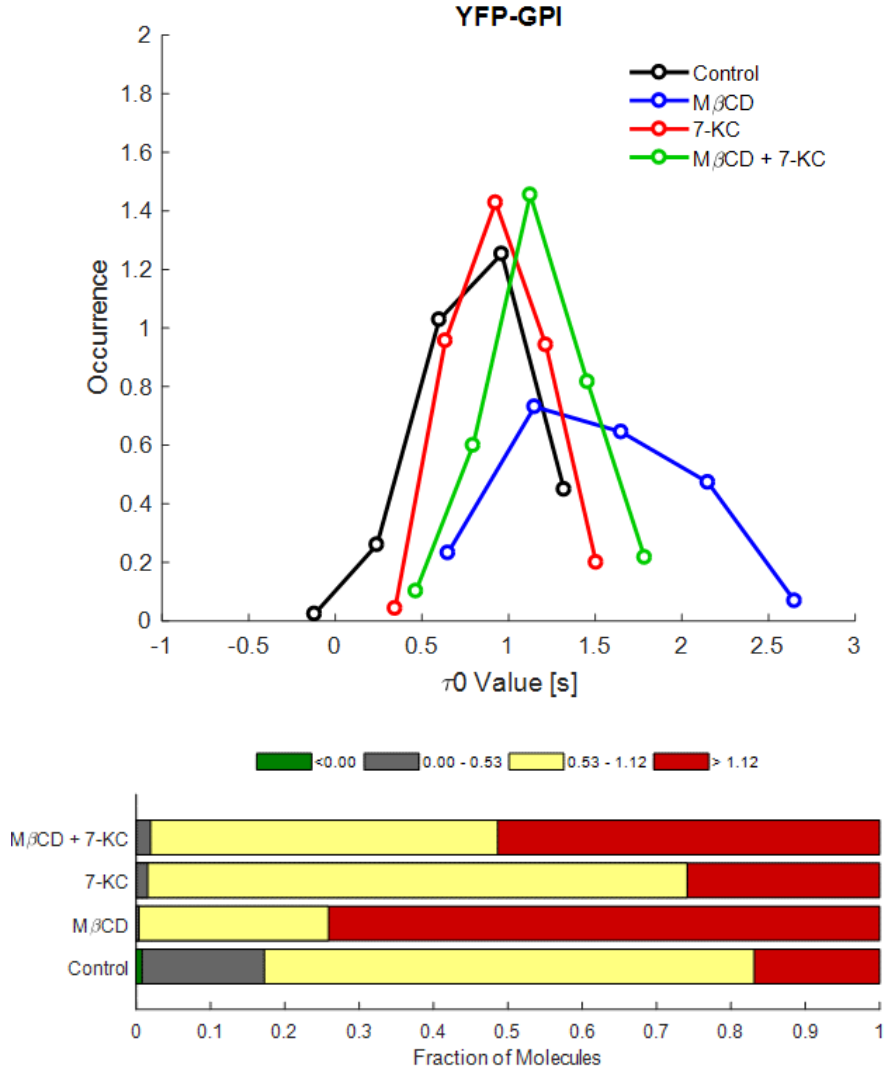

Figure 12. Effects of Cholesterol Depletion & 7-KC Addition on YFP-GPI τ_0 Distributions

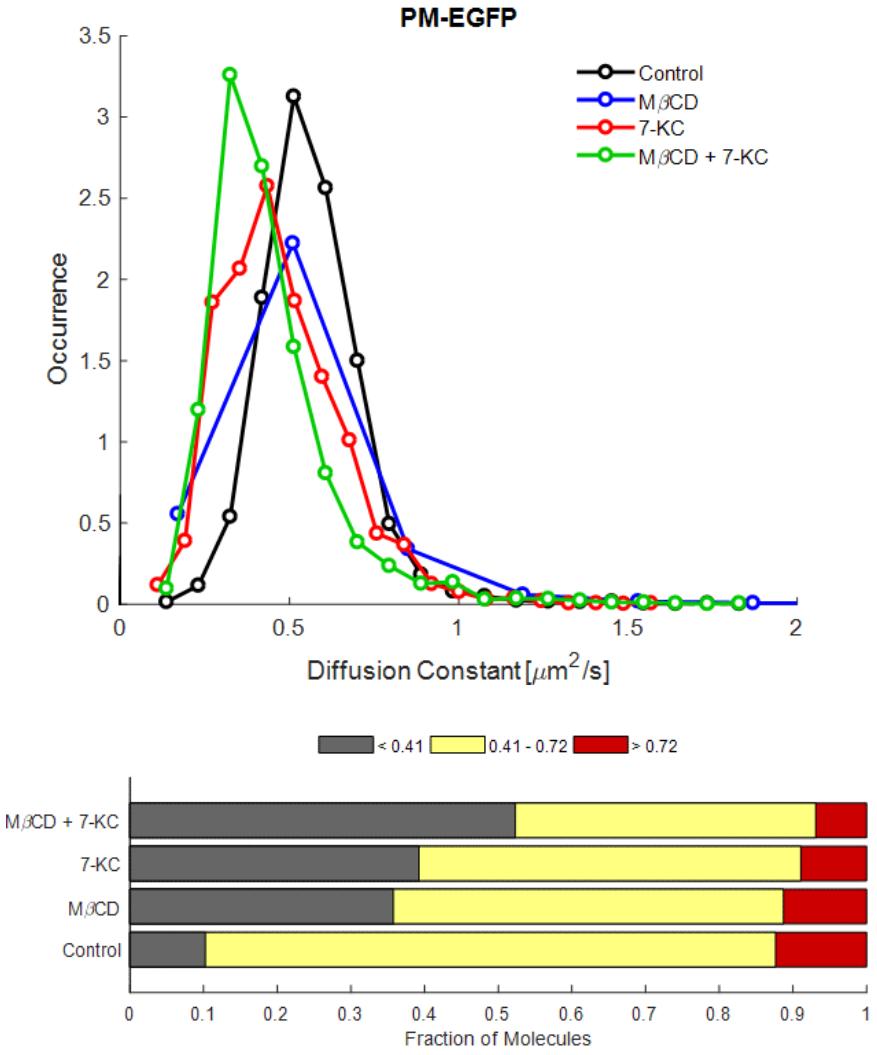

Figure 13. Effects of Cholesterol Depletion & 7-KC Addition on PM-EGFP D Distributions

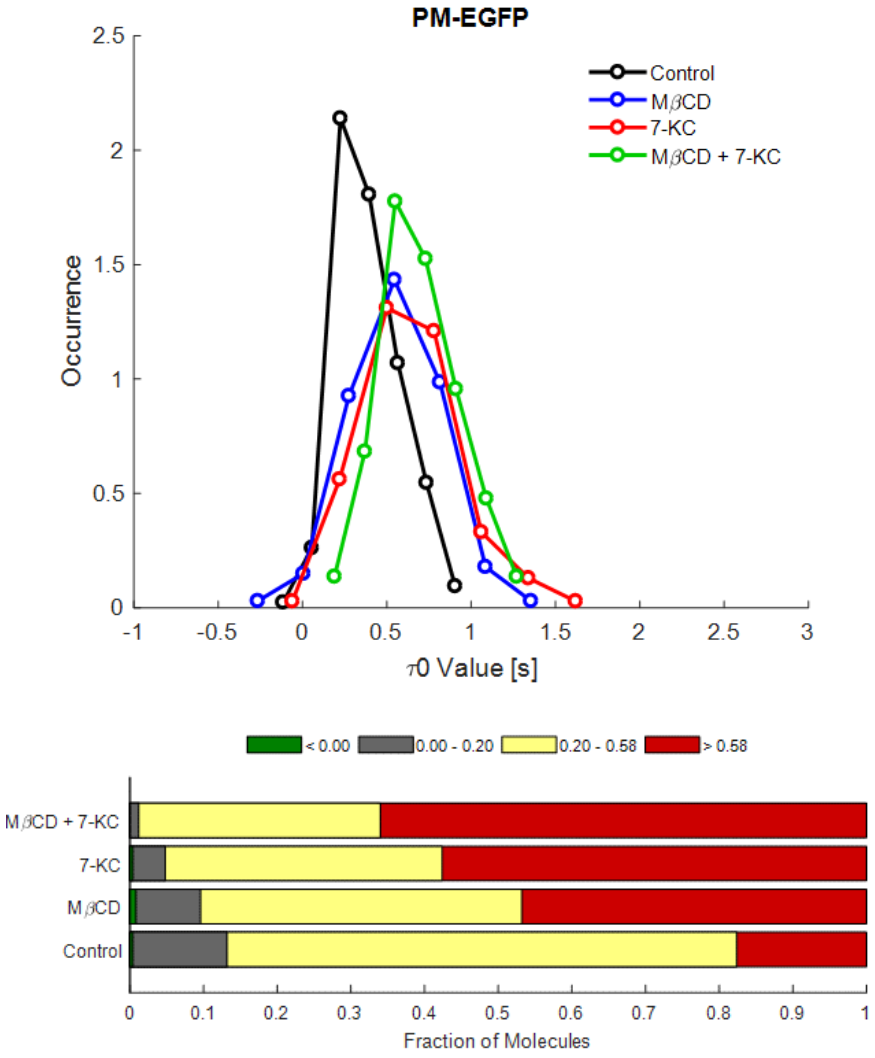

Figure 14. Effects of Cholesterol Depletion & 7-KC Addition on PM-EGFP τ_0 Distributions

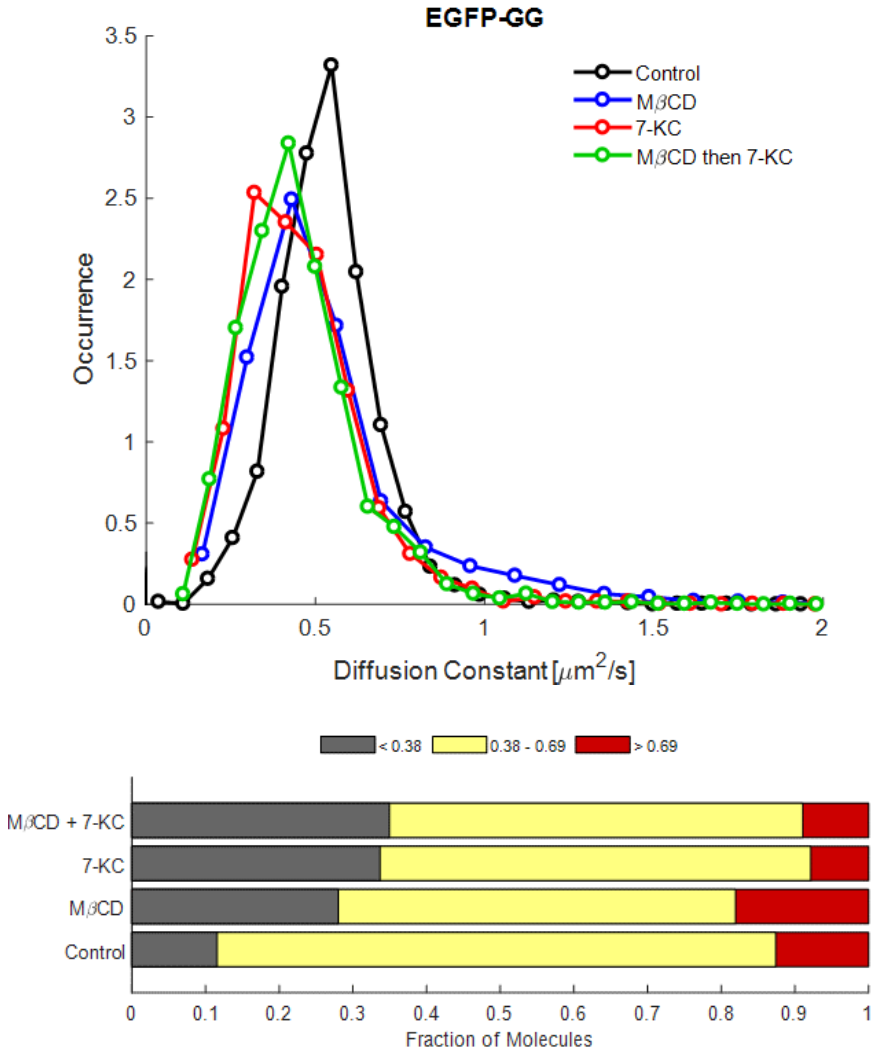

Figure 15. Effects of Cholesterol Depletion & 7-KC Addition on EGFP-GG D Distributions

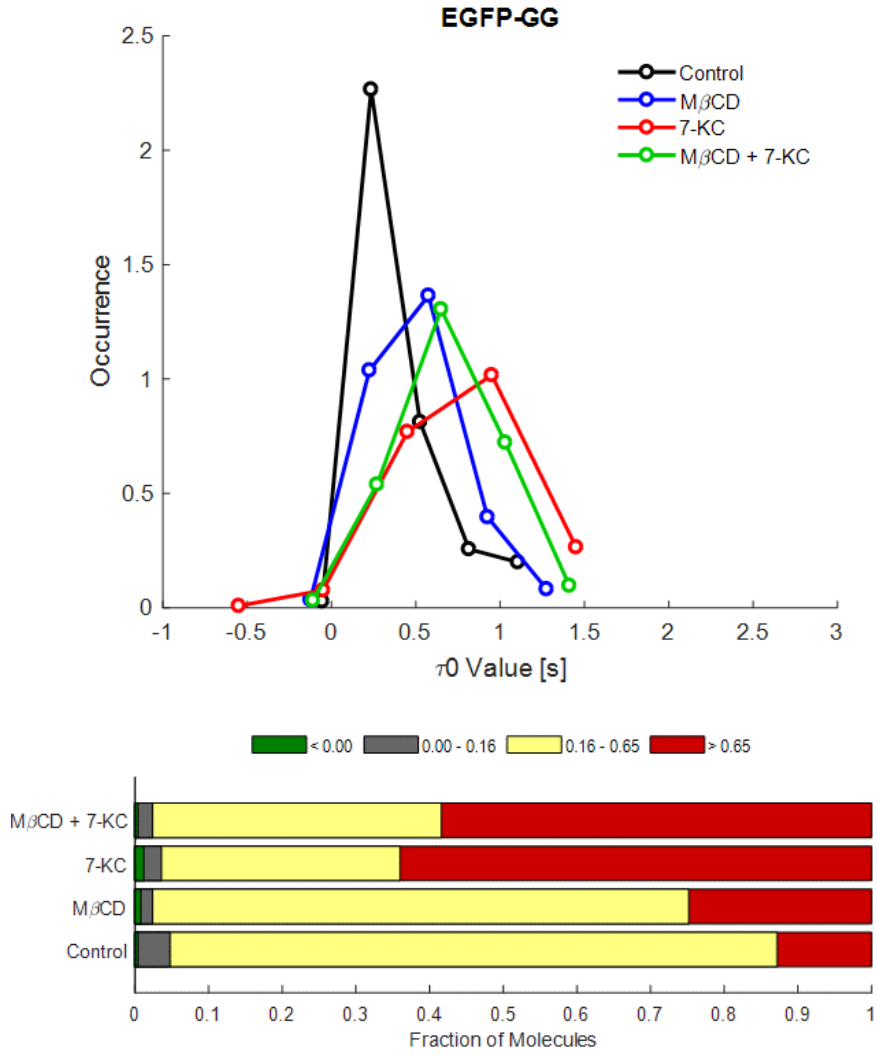

Figure 16. Effects of Cholesterol Depletion & 7-KC Addition on EGFP-GG τ_0 Distributions

Effects of Cytochalasin D

on Inner and Outer Leaflet Lo / Ld Fluorescent Reporters

Lastly, to assess the role of the actin cytoskeleton in controlling lipid ordering indicated by these fluorescent probes, actin polymerization was inhibited by incubation with 2 μM CytoD for 5 minutes at room temperature. No significant change for either D or τ_0 values obtained for YFP-GPI (Figures 17 & 18). However, PM-EGFP expressed a significant increase in the fraction of slow D and long transient confinement time as shown by the normalized distribution of these values (Figures 21 & 22). These effects were not observed for EGFP-GG, but rather a broadening of these distributions was found (Figures 23 & 24). Also, unlike that of EGFP-GG, a substantial increase in the fraction of EGFP-GG molecules exhibiting hop diffusion (Figure 22, green bar) was also found. Data are summarized in Table 3.

Protein	Treatment	Diffusion Constant (μm^2/ s)	$\tau 0$ (s)	# of Cells	# of Samples
YFP-GPI	Control	0.37 ± 0.19	0.84 ± 0.34	9	2
	CytoD	0.39 ± 0.20	0.86 ± 0.33	10	2
PM-EGFP	Control	0.63 ± 0.15	0.30 ± 0.18	9	2
	CytoD	0.55 ± 0.14	0.43 ± 0.19	10	2
EGFP-GG	Control	0.66 ± 0.25	0.25 ± 0.19	10	2
	CytoD	0.63 ± 0.29	0.29 ± 0.17	10	2

Table 3. Summary of average results obtained from imaging FCS measurements on resting RBL-2H3 cells incubated with 2 μM CytoD in Tyrodes buffer solution.

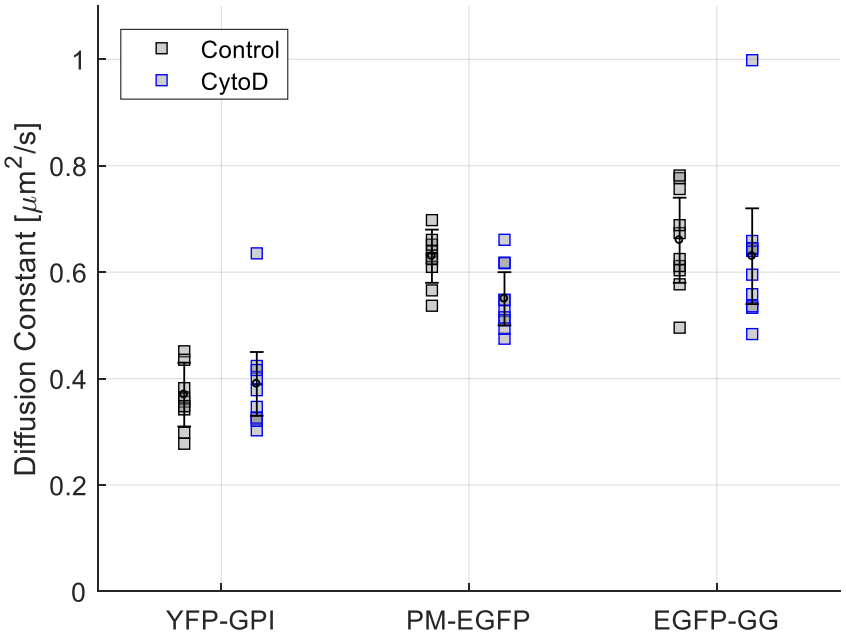

Figure 17. Effects of CytoD on D Averages

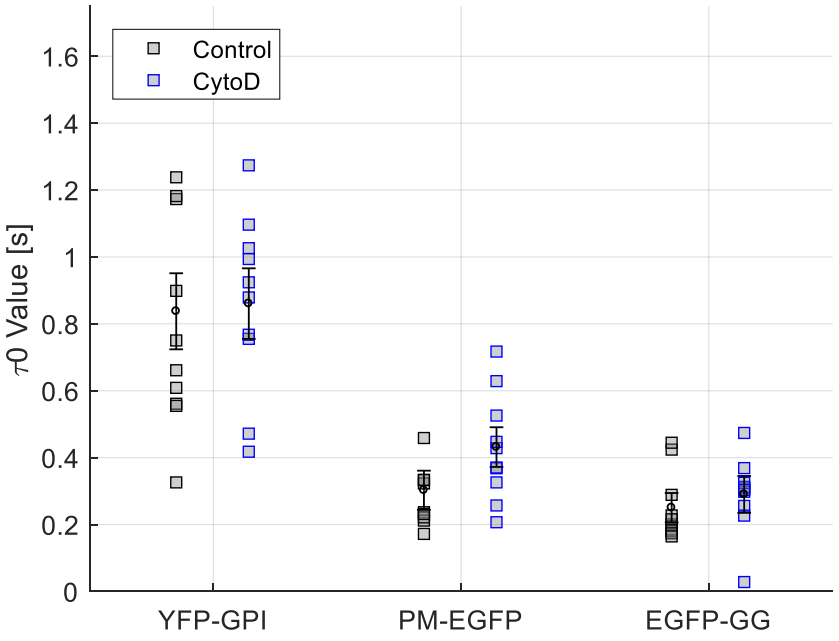

Figure 18. Effects of CytoD on τ_0 Averages

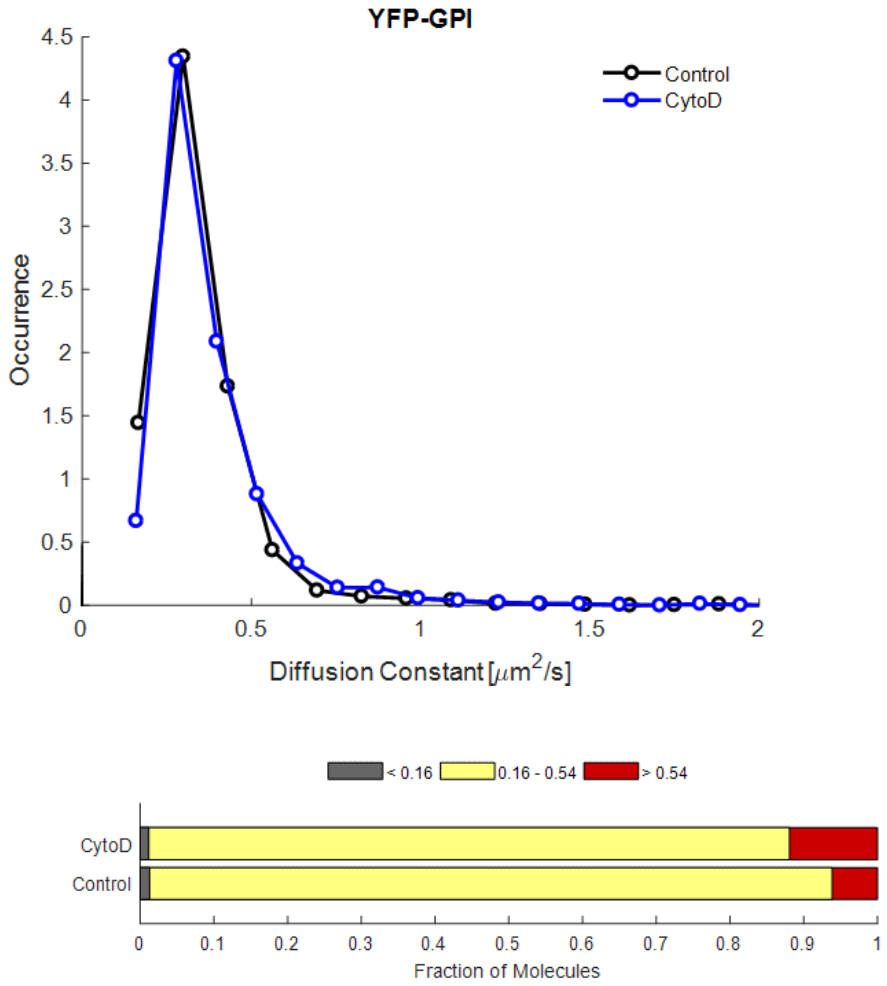

Figure 19. Effects of CytoD on YFP-GPI D Distributions

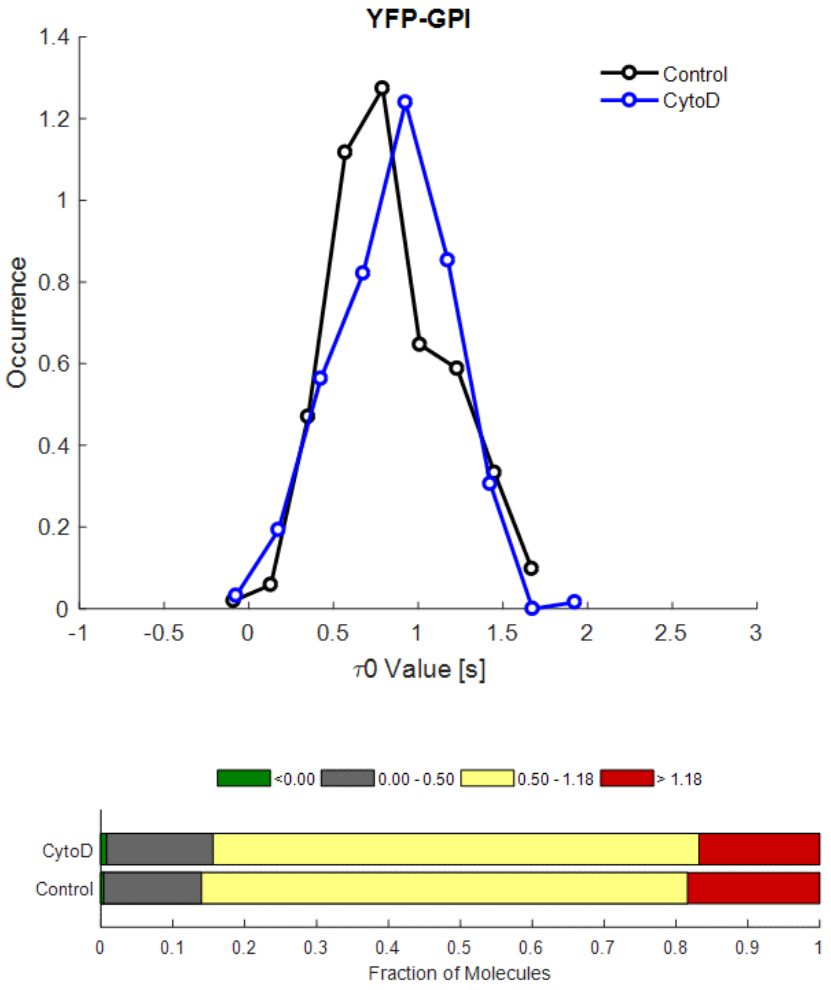

Figure 20. Effects of CytoD on YFP-GPI τ_0 Distributions

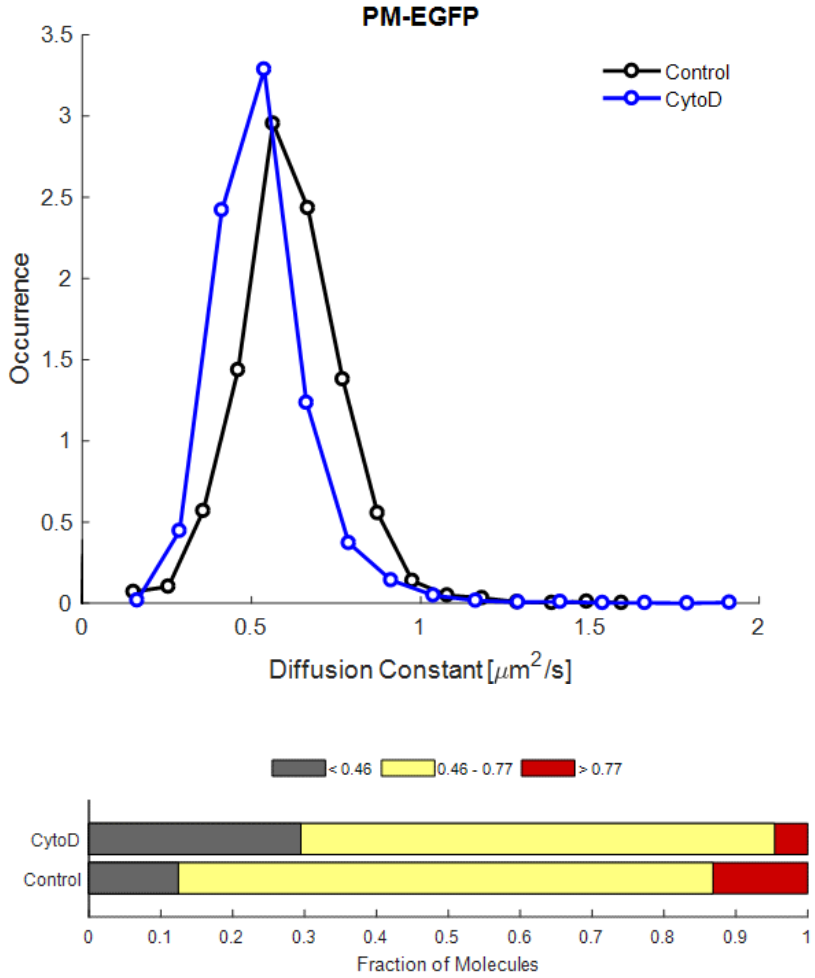

Figure 21. Effects of CytoD on PM-EGFP D Distributions

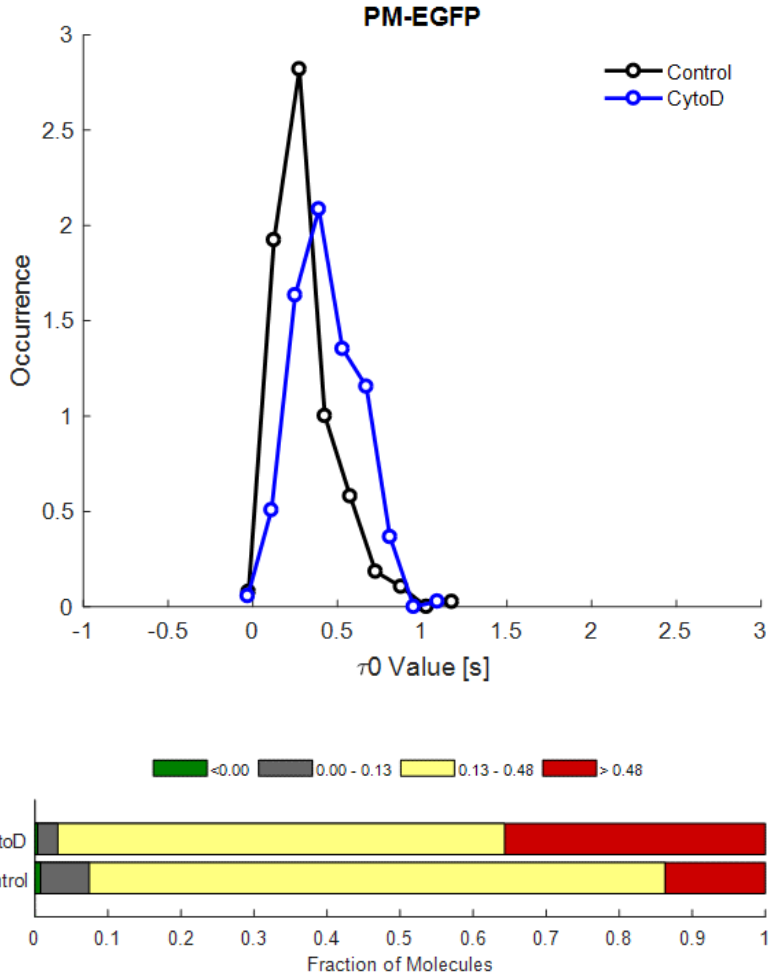

Figure 22. Effects of CytoD on PM-EGFP τ_0 Distributions

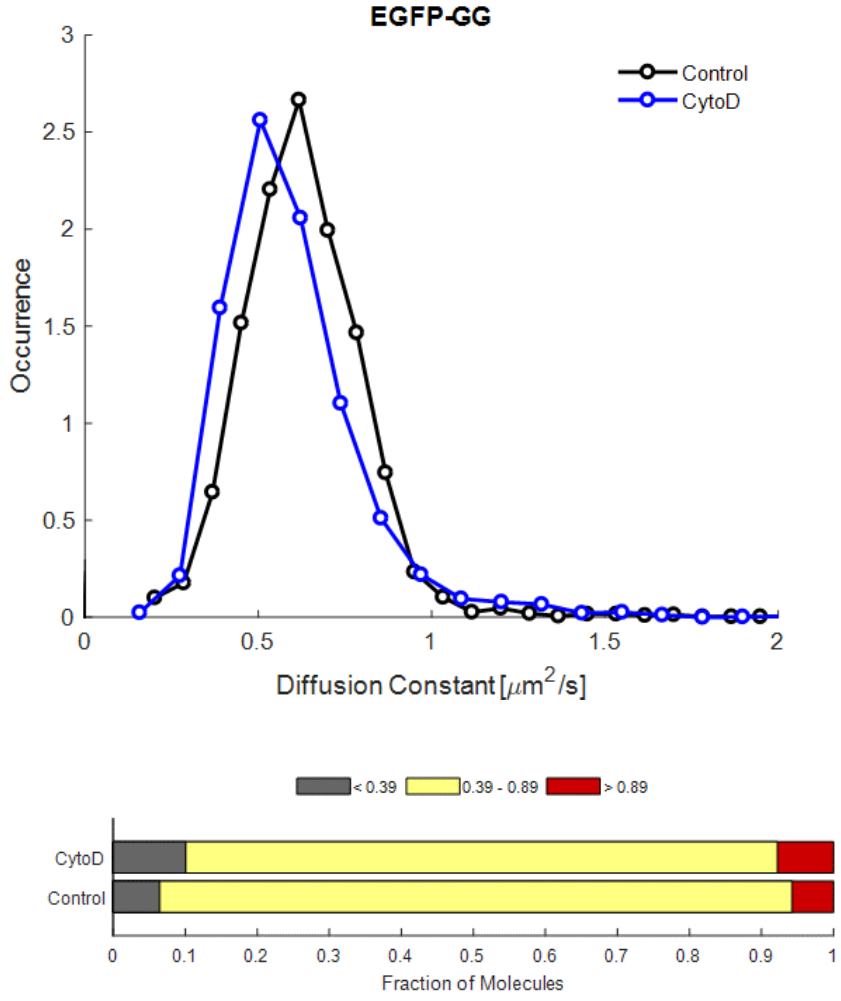

Figure 23. Effects of CytoD on EGFP-GG D Distributions

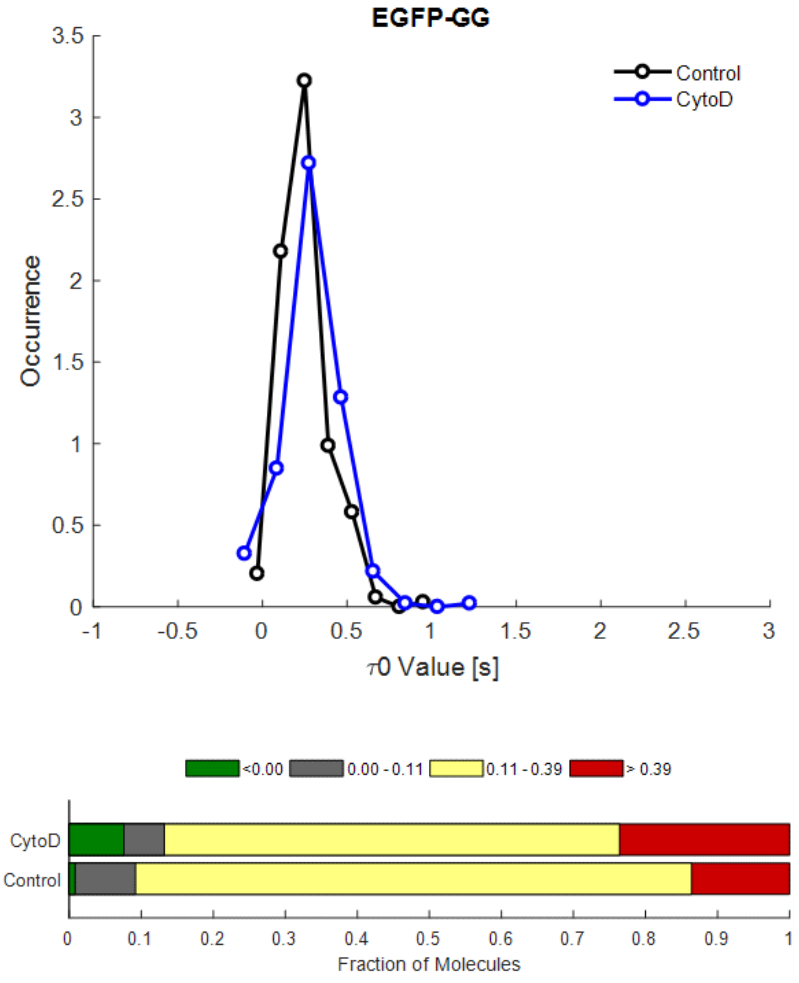

Figure 24. Effects of CytoD on EGFP-GG τ_0 Distributions

DISCUSSION

The results from the present study provide experimental evidence of the relative effect of which a variety of pharmacological perturbations have on the inner- and outer- leaflets of the RBL-2H3 cell lipid bilayer. Each of these treatments, which include exogenous addition of short-chain ceramides, MβCD, 7-KC, and Cytochalasin D (CytoD), were implemented in efforts to identify a potential treatment which would render L_o-like regions of the resting RBL-2H3 cell membrane into that of L_d for further study on the role of these hypothesized domains in relation to IgE high affinity receptor FcεRI signaling. A significant body of work has been developed in regard to these various treatments which provides ample background and reasoning for their implementation in this study which will be referenced throughout this discussion.

Sphingolipids play a substantial role in constituting the lipid bilayer and have been shown to be biologically active signaling molecules (Okazaki et al., 1989). By action of sphingomyelinase, sphingomyelin located at the plasma membrane is hydrolyzed to render ceramide which has been indicated in regulating a plethora of biological processes including mediation of immune response (Kolesnick et al., 2002). The chemical structure of ceramides is that of a sphingosine backbone covalently attached to a fatty acid of varying acyl chain length via an amide bond. In order to perturb the effect of endogenous, long-chain ceramides induced to be present at the plasma membrane, cell permeable short-chain, (C2-C6 fatty acid acyl chain) ceramides are used. Previous work in the Baird-Holowka laboratory has shed light on the ability of exogenous addition of short-chain ceramides in generating disorder at the lipid bilayer in-vitro and in-vivo. Steady-state fluorescence anisotropy measurements of membrane vesicles extracted from RBL-2H3 cells have shown evidence of the lipid disordering capability of C2- and C6- ceramide where C6-ceramide was more potent in

decreasing anisotropy (which means a more disordered nature of the plasma membrane) when compared to that of C2-ceramide. In the same study, C2- and C6- ceramide were found to disrupt raft structure in-vivo as indicated by Förster resonance energy transfer (FRET) where it was found that both C2- and C6- ceramide decreased FRET between Cy3-labeled anti-Thy1 bound Thy1 (GPI-anchored ordered region marker) and Alexa488-IgE bound FcεRI indicating their ability to disrupt L_o-like region structure (Gidwani et al., 2003). These observations encouraged us to use short chain ceramides as potential candidates for Imaging FCS measurements to test the modulations of plasma membrane organization.

In the present context of measurements conducted by imaging FCS, exogenous addition of C2- ceramide resulted in transbilayer asymmetric effects between L_o-like region preferring fluorescent reporters on either leaflet of the lipid bilayer. While diffusion remained unchanged for outer-leaflet marker, YFP-gl-GPI, the distribution of PM-EGFP exhibits increased variability. In addition, there exists no significant change in transient confinement time for PM-EGFP while that of YFP-gl-GPI decreases. These findings suggest that C2-ceramide treatment by exogenous addition to resting RBL-2H3 cells does not affect L_o-like regions of the lipid monolayers at the plasma membrane in proportion to one another. Rather, C2-ceramide disorders outer-leaflet L_o-like domains as shown by a decrease in transient confinement time of YFP-GPI, but does not change lipid order for inner-leaflet L_o-like regions. It is not likely that this is attributed to C2-ceramide being localized solely at outer-leaflet L_o-like domains as the probability of C2-ceramide transbilayer movement is high. It is more probable that these asymmetric trends are an expression of the difference in phospholipid species and cholesterol content which inherently exists between lipid monolayers in-vivo. Short and long acyl chain ceramides have previously been shown to exclude cholesterol from cholesterol-dependent L_o-like domains in-vitro (Megha & London, 2004; Schwille et al.,

2006). Although the exact location(s) of cholesterol at the plasma membrane is controversial, recent experimental evidence of cholesterol occupying a lower mole fraction at the cytoplasmic face of the lipid bilayer has been found in HeLa cells using orthogonal lipid sensors (Liu et al., 2017). The lack of change in order as indicated by transient confinement time of PM-EGFP under C2-ceramide treatment conditions may be caused by this lack of cholesterol content at the cytoplasmic face of the membrane in RBL-2H3 cells. This lack of change in order as indicated by PM-EGFP transient confinement is reinforced by data collected for C6-ceramide treatments, despite its increased potency for lipid disorder inducing effects on a mole-per-mole basis compared to that of C2-ceramide for outer-leaflet L_o-like region marker YFP-GPI. Clearly, there exists a coupling between monolayers as indicated by the symmetric increase in diffusion constants obtained for treatment with C6-ceramide on outer- and inner-leaflet fluorescent reporters despite asymmetric lipid disordering effects. It is likely that this coupling in diffusion for these domain markers is caused by the high rate of flip-flop of C6-ceramide between the two monolayers. In combination, these data support the perspective of short-chained ceramides increasing membrane fluidity rather symmetrically between lipid monolayers while the disordering effects may be localized to the outer-leaflet possibly due to a higher abundance of sterols located at the outer-leaflet (and thus a higher fraction of ordered regions at the outer leaflet in unperturbed cells). To further investigate this discrepancy between monolayers, the effects of C6-ceramide integration on the plasma membrane were observed directly for transmembrane protein Alexa488-IgE-FcεRI. Intriguingly, C6-ceramide caused no increase in lateral diffusion constants compared that of the control, while still inducing a decrease in transient confinement time. The lack of change in diffusion is likely caused by the substantial increase in mass and volume of which the FcεRI complex contains / occupies compared to that of the GPI anchor and palmitate-myristate anchor of YFP-GPI and PM-EGFP respectively. The magnitude of reduction in

order of the local lipid environment for FcεRI is similar to that found for YFP-GPI (~11% and ~16% reduction in average τ_0 value respectively) is predominantly influenced by C6-ceramides ability to disorder outer-leaflet L_o-like regions as previously discussed.

Methyl-beta-cyclodextrin (MβCD) is a common drug used for cholesterol depletion at the plasma membrane. These oligosaccharide heptamers are structurally cyclical, and have the highest affinity for cholesterol at their hydrophobic core in comparison to their α and γ counterparts (Pitha et al., 1989). Previous work in the Baird-Holowka laboratory has shown a loss of association of both Lyn kinase and cross-linked FcεRI with DRMs isolated after TritonX-100 treatment and decreased tyrosine phosphorylation of FcεRI by Lyn kinase suggesting the criticality of their localization in cholesterol-dependent L_o-like domains for initial steps in FcεRI signaling (Sheets, Holowka, & Baird, 1999). The effect of MβCD on the three fluorescent reporters used in this study sheds light on the consequences of cholesterol depletion on lipid order and fluidity in-vivo. Under a cholesterol depleted lipid environment induced by MβCD, there is global increase in transient confinement exhibited by both L_o inner- and outer-leaflet reporters as well as L_d preferring inner-leaflet reporter EGFP-GG. This provides evidence for a global increase in gel-like lipid phase caused by cholesterol depletion at the membrane of RBL-2H3 cells. These results are surprising, considering a previous in-vivo FCS study which has been conducted using other cell types which show the expected decrease in lipid order as result of cholesterol removal from L_o regions (Bag, Huang, & Wohland, 2015). The cause of such a result is not fully understood, but this increase in order indicated by these membrane anchored probes may be cell line dependent (Huang et al., 2016), perhaps even unique to the RBL-2H3 plasma membrane. Intuitive to increased confinement time is the decrease in diffusion constants found for L_o-like region reporters. However, this change is not exhibited for EGFP-GG, but rather a broadened

distribution of D. The implications of this result are unclear, although it is likely that inner-leaflet lipid reorganization by cholesterol depletion results in a less structurally accommodating local lipid environment, expunging the sterically hindered geranylgeranyl anchor of this probe from partitioning into these newly formed domains.

7-ketocholesterol (7-KC) is an oxysterol derivative of cholesterol which has been shown to intercalate into L_o-like regions of membranes in-vitro by analysis of DRM yield (Massey & Pownall, 2005). The disordering properties of 7-KC, namely their ability to convert L_o regions to that of L_d has been demonstrated in Jurkat-derived T cells and HeLa cells by generalized polarization of Laurdan labeled cells and fluorescence-lifetime imaging microscopy (FLIM)-FCS respectively (Gaus et al. 2012; Rentero et al., 2008). The results found in this study provide contrasting evidence despite following the same methodology for exogenous addition of 7-KC to resting cells. Just as in the case of cholesterol depletion, a global increase in long transient confinement time was found while effects to diffusion constants differed between inner- and outer-leaflet probes indicative of increased lipid order rather than the expected decrease. The discrepancy between the membrane disordering effects reported for 7-KC addition and the results presented in this study are difficult to reconcile. However, these results do support the notion that the RBL-2H3 membrane exhibits unusual characteristics compared to other cell lines. Due to the increased polarity of 7-KC and its decreased packing efficiency, 7-KC has been shown to have a rate of translocation between lipid monolayers orders of magnitude faster than cholesterol (Vila et al., 2001). Therefore, it is not likely that the overall increase in membrane order / decreased fluidity of inner-leaflet probes is due to fixed localization of 7-KC at the inner-leaflet although it cannot be ruled out that it may exist in higher molar ratios at the inner-leaflet under these treatment conditions. In fact, recent experimental evidence suggests exogenous addition of cholesterol

to the plasma membrane of HeLa cells is asymmetrically distributed resulting in no significant increase in cholesterol found at the outer-leaflet, but a 73% increase of inner-leaflet cholesterol (Liu et al., 2017). Hence, the asymmetric effects observed by 7-KC addition between leaflets may be due to the method of delivery to the plasma membrane by MβCD rather than a lack in the ability for 7-KC to induce symmetric effects if delivered efficiently to both lipid monolayers using a different approach.

The contrast between outer- and inner-leaflet probes under 7-KC addition spurred inquiry of whether 7-KC affected the relative abundance of cholesterol between monolayers which could possibly perturb lipid order. Therefore, a combination of treatments was used first by incubating with MβCD for cholesterol depletion and then 7-KC addition. Under these conditions, a restorative effect towards, although not reaching, control diffusion and transient confinement time was observed for YFP-GPI. This reinforces evidence found regarding 7-KC occupancy of ordered lipid environments in-vivo. Additionally, these results provide a context in which 7-KC induces disorder at the outer-leaflet, namely, after new domains form by cholesterol depletion. This combination of treatments provided an even larger fraction of PM-EGFP molecules exhibiting long-time transient confinement while less was found for EGFP-GG. These findings lend aid to the notion that it is 7-KC itself that induces increased lipid order and that its interactions with phospholipids at these ordered regions enables this condensation.

Due to the cytoskeleton's role in actively regulating membrane fluidity and lipid organization at the plasma membrane, CytoD was tested. CytoD is a common pharmacological treatment for inhibiting active actin polymerization in-vivo by its ability to arrest polymerization at the barbed end of actin filaments (Cooper, 1987). No evidence of change was observed for YFP-GPI under actin inhibited conditions, although statistically

significant change was observed for PM-EGFP and to a lesser extent EGFP-GG. The lack in difference between treated and control for YFP-GPI agrees with previous FCS measurements of COS-7 cells observing GFP-GPI under these same treatment conditions (Lenne et al. 2006). In contrast to the outer-leaflet, the increased order induced at the inner leaflet for both L_o and L_d markers provides evidence for the actin cytoskeleton's role at regulating inner-leaflet membrane order. The significant increase in transient confinement by PM-EGFP compared to that of EGFP-GG lends further evidence to the notion that the cytoskeleton is localized at ordered regions (Wu et al., 2004). Data for PM-EGFP under CytoD treatment conditions suggest an increase in local lipid order, although reasons for this remain unclear considering the opposite effect has been found for inhibition of actin polymerization by CytoD using other L_o-like fluorescent reports in other cell types (Adkins et al. 2007).

The body of evidence provided in this study by imaging FCS measurements does not implicate the majority of the employed pharmacological perturbations to be effective at disrupting L_o-like regions on the resting RBL-2H3 membrane. Rather, these perturbations often indicated an increase in phospholipid order to some degree although this effect varied depending on the targeted lipid environment by these fluorescent reporters. However, C2 and C6-ceramides were found to disrupt outer-leaflet L_o-like regions, with C6-ceramide being more effective on a mole-per-mole basis. The results of this study also highlight the asymmetry of effects exhibited by these treatments between L_o-like regions of lipid monolayers in-vivo, which may have implications for findings regarding IgE receptor-mediated signaling when observed using similar treatment conditions.

The root cause of increased lipid order by these treatments in RBL-2H3 cells, contrary to the expected and experimentally demonstrated decrease in lipid order in other models,

remains to be determined. Further insights might be gathered by changing the pharmacological perturbations used to reach a similar desired effect. For instance, in this study MβCD was used to directly extract and deplete the membrane of cholesterol in-vivo, but a similar effect could possibly be achieved by inhibition of de novo synthesis of cholesterol in the RBL-2H3 cell by other drugs such as mevastatin. In this way, pleiotropic effects by MβCD may be identified when compared. As lipid phase properties are largely controlled by cholesterol content it would be desirable to monitor cholesterol content between leaflets under these various conditions perhaps by means of fluorescently labeled cholesterol in combination with fluorescence quenchers.

APPENDIX A - MATLAB CODE FOR MULTIPLE WEIGHTED LEAST SQUARES (WLS) REGRESSION

In order save significant time during analysis, the following MATLAB code was developed to automate the acquisition of the intercept values (τ_0) from the diffusion law over sub-regions of the image.

"ImFCS" plugin for FIJI was used to produce the excel sheets containing data consisting of τ_D values for each iteration of binning (2-5) within the ROI.

This MATLAB code enables a linear fitting and storage of τ_0 values using WLS where the weights are 1/SEM from these excel files.

The SEM is calculated by extracting standard deviation values provided by "ImFCS" software, and allows the user to enter the number of observations (N) which depends on the ROI and pixel area of the .TIFF image stack.

```
xlfile_dir=uigetdir;
cd(xlfile_dir);
dir_vec=dir([xlfile_dir, '\*.xlsx']);%generate vector of directory .xslx files
filenames = {dir_vec(:).name}.';%file names must have same number of characters

for i = 1:length(dir_vec(:))
      fullname = [xlfile_dir filesep dir_vec(i).name];
Excel = actxserver('excel.application');
Excel.workbooks.Open(fullname,0,true);
sheets=Excel.ActiveWorkBook.Sheets;
sheetdifflaw=get(sheets,'Item',20);
sheetdifflaw.Activate;
nCols = Excel.ActiveSheet.UsedRange.Columns.Count;
nRows = Excel.ActiveSheet.UsedRange.Rows.Count;
Excel.Quit
Excel.delete
pause(0.1);
tksc(i,:)=char(filenames(i));
[num]=xlsread(tksc(i,:),'DiffLaw Map SD');
v=1:nCols-1;%iterates through column count for DiffLaw Map SD
stdeviation=num(:,v);
Nvalue=[, , , ,]; %Comma separated list of N's in decreasing order from left to right provided by user (for 1-
5 binning)
        for kdx=1:5
        weight(kdx,v)=(stdeviation(kdx,v)./(Nvalue(kdx)).^0.5).^-1;
        end
[tt]=xlsread(tksc(i,:),'DiffLaw Map Data');
x=tt(2:5,1);%extracts single column vector for x (2-5 binning)
j=2:nCols;
y=tt(2:5,j);%array for all y-intercepts
s=sum(weight(2:5,v));
sx=sum(weight(2:5,v).*x);
sy=sum(weight(2:5,v).*y);
sxx=sum(weight(2:5,v).*x.^2);
sxy=sum(weight(2:5,v).*x.*y);
delta=s.*sxx-(sx).^2;
a=(sxx.*sy-sx.*sxy)./delta;
b=(s.*sxy-sx.*sy)./delta;
Results.slope=b;%generate construct containing all calculated slopes
Results.Intercept=a;%generate construct containing all calculated y-intercepts
y_fit=a+b.*x;
 resizea=a(:);
 vec{i}=resizea;
End
```

REFERENCES

Adkins, E. M., Samuvel, D. J., Fog, J. U., Eriksen, J., Jayanthi, L. D., Vaegter, C. B., ... & Gether, U. (2007). Membrane mobility and microdomain association of the dopamine transporter studied with fluorescence correlation spectroscopy and fluorescence recovery after photobleaching. *Biochemistry*, *46*(37), 10484-10497.

BAG, N. (2014). *Imaging fluorescence correlation spectroscopy studies lipid membrane dynamics and organization: Applications to the investigation of lipid bilayers, cell membranes, and membrane active peptides* (Doctoral dissertation).

Bag, N., Huang, S., & Wohland, T. (2015). Plasma Membrane Organization of Epidermal Growth Factor Receptor in Resting and Ligand-Bound States. *Biophys J*, *109*(9), 1925–1936. https://doi.org/10.1016/j.bpj.2015.09.007

Bag, N., Ng, X. W., Sankaran, J., & Wohland, T. (2016). Spatiotemporal mapping of diffusion dynamics and organization in plasma membranes. *Methods and Applications in Fluorescence*, *4*(3), 034003.

Bai, J., & Pagano, R. E. (1997). Measurement of spontaneous transfer and transbilayer movement of BODIPY- labeled lipids in lipid vesicles. *Biochemistry*, *36*(29), 8840–8848. https://doi.org/10.1021/bi970145r

Baumgart, T., Hammond, A. T., Sengupta, P., Hess, S. T., Holowka, D. A., Baird, B. A., & Webb, W. W. (2007). Large-scale fluid/fluid phase separation of proteins and lipids in giant plasma membrane vesicles. *Proceedings of the National Academy of Sciences*, *104*(9), 3165–3170. https://doi.org/10.1073/pnas.0611357104

Brown, D. A., & London, E. (1997). Structure of detergent-resistant membrane domains: Does

phase separation occur in biological membranes? *Biochemical and Biophysical Research Communications*, *240*(1), 1–7. https://doi.org/10.1006/bbrc.1997.7575

Brown, D. A., & Rose, J. K. (1992). Sorting of GPI-anchored proteins to glycolipid-enriched membrane subdomains during transport to the apical cell surface. *Cell*, *68*(3), 533-544.

Chen, L., Yu, Z., & Quinn, P. J. (2007). The partition of cholesterol between ordered and fluid bilayers of phosphatidylcholine: A synchrotron X-ray diffraction study. *Biochimica et Biophysica Acta - Biomembranes*, *1768*(11), 2873–2881. https://doi.org/10.1016/j.bbamem.2007.07.023

Chiantia, S., Kahya, N., Ries, J., & Schwille, P. (2006). Effects of ceramide on liquid-ordered domains investigated by simultaneous AFM and FCS. *Biophysical Journal*, *90*(12), 4500–4508. https://doi.org/10.1529/biophysj.106.081026

Collins, M. D. (2008). Interleaflet coupling mechanisms in bilayers of lipids and cholesterol. *Biophysical Journal*, *94*(5), 32–34. https://doi.org/10.1529/biophysj.107.124362

Collins, M. D., & Keller, S. L. (2008). Tuning lipid mixtures to induce or suppress domain formation across leaflets of unsupported asymmetric bilayers. *Proceedings of the National Academy of Sciences*, *105*(1), 124–128. https://doi.org/10.1073/pnas.0702970105

Contreras, F. X., Sánchez-Magraner, L., Alonso, A., & Goñi, F. M. (2010). Transbilayer (flip-flop) lipid motion and lipid scrambling in membranes. *FEBS Letters*, *584*(9), 1779–1786. https://doi.org/10.1016/j.febslet.2009.12.049

Cooper, J. A. (1987). Effects of cytochalasin and phalloidin on actin. *The Journal of cell biology*, *105*(4), 1473-1478.

Cremesti, A. E., Goni, F. M., & Kolesnick, R. (2002). Role of sphingomyelinase and ceramide in modulating rafts: Do biophysical properties determine biologic outcome? *FEBS*

Letters, *531*(1), 47–53. https://doi.org/10.1016/S0014-5793(02)03489-0

Davey, A. M., Walvick, R. P., Liu, Y., Heikal, A. A., & Sheets, E. D. (2007). Membrane order and molecular dynamics associated with IgE receptor cross-linking in mast cells. *Biophysical Journal*, *92*(1), 343–355. https://doi.org/10.1529/biophysj.106.088815

De Almeida, R. F. M., Loura, L. M. S., Fedorov, A., & Prieto, M. (2005). Lipid rafts have different sizes depending on membrane composition: A time-resolved fluorescence resonance energy transfer study. *Journal of Molecular Biology*, *346*(4), 1109–1120. https://doi.org/10.1016/j.jmb.2004.12.026

Devaux, P. F., & Morris, R. (2004). Transmembrane asymmetry and lateral domains in biological membranes. *Traffic*, *5*(4), 241–246. https://doi.org/10.1111/j.1600-0854.2004.0170.x

Fadeel, B., & Xue, Di. (2009). Membrane Asymmetry : Roles in Health and Disease. *Crit Rev Biochem Mol Biol*, *44*(5), 264–277. https://doi.org/10.1080/10409230903193307.The

Feigenson, G. W. (2009). Phase diagrams and lipid domains in multicomponent lipid bilayer mixtures. *Biochimica et Biophysica Acta - Biomembranes*, *1788*(1), 47–52. https://doi.org/10.1016/j.bbamem.2008.08.014

Fridriksson, E. K., Shipkova, P. A., Sheets, E. D., Holowka, D., Baird, B., & McLafferty, F. W. (1999). Quantitative analysis of phospholipids in functionally important membrane domains from RBL-2H3 mast cells using tandem high-resolution mass spectrometry. *Biochemistry*, *38*(25), 8056-8063.

Frye, L. D., & Edidinf, M. (n.d.). THE RAPID INTERMIXING OF CELL SURFACE ANTIGENS AFTER FORMATION OF MOUSE-, 319–336.

Fujiwara, T., Ritchie, K., Murakoshi, H., Jacobson, K., & Kusumi, A. (2002). Phospholipids undergo hop diffusion in compartmentalized cell membrane. *Journal of Cell Biology*,

157(6), 1071–1081. https://doi.org/10.1083/jcb.200202050

Garg, S., Rühe, J., Lüdtke, K., Jordan, R., & Naumann, C. A. (2007). Domain registration in raft-mimicking lipid mixtures studied using polymer-tethered lipid bilayers. *Biophysical Journal*, *92*(4), 1263–1270. https://doi.org/10.1529/biophysj.106.091082

Gidwani, A., Brown, H. A., Holowka, D., & Baird, B. (2003). Disruption of lipid order by short-chain ceramides correlates with inhibition of phospholipase D and downstream signaling by FcepsilonRI. *Journal of Cell Science*, *116*, 3177–3187. https://doi.org/10.1242/jcs.00621

Guasto, J. S., Huang, P., & Breuer, K. S. (2008). Evanescent Wave Illumination. *Encyclopedia of Micro- and Nano-Fluidics*, 638–644.

Gurunadh R. Chichili and William Rodgers. (2010). NIH Public Access. *Cell Mol Life Sci*, *66*(14), 2319–2328. https://doi.org/10.1007/s00018-009-0022-6.Cytoskeleton-Membrane

Heerklotz, H. (2002). Triton promotes domain formation in lipid raft mixtures. *Biophysical Journal*, *83*(5), 2693–2701. https://doi.org/10.1016/S0006-3495(02)75278-8

Holowka, D., Gosse, J. A., Hammond, A. T., Han, X., Sengupta, P., Smith, N. L., … Baird, B. (2005). Lipid segregation and IgE receptor signaling: A decade of progress. *Biochimica et Biophysica Acta - Molecular Cell Research*, *1746*(3), 252–259. https://doi.org/10.1016/j.bbamcr.2005.06.007

Holowka, D., Sheets, E. D., & Baird, B. (2000). Interactions between Fc(epsilon)RI and lipid raft components are regulated by the actin cytoskeleton. *Journal of Cell Science*, *113 (Pt 6*, 1009–1019.

Huang, S., Lim, S. Y., Gupta, A., Bag, N., & Wohland, T. (2016). Plasma membrane organization and dynamics is probe and cell line dependent. *Biochimica et Biophysica Acta (BBA)-Biomembranes*.

Ingólfsson, H. I., Melo, M. N., Van Eerden, F. J., Arnarez, C., Lopez, C. A., Wassenaar, T. A., … Marrink, S. J. (2014). Lipid organization of the plasma membrane. *Journal of the American Chemical Society*, *136*(41), 14554–14559. https://doi.org/10.1021/ja507832e

Kahya, N., Scherfeld, D., Bacia, K., Poolman, B., & Schwille, P. (2003). Probing lipid mobility of raft-exhibiting model membranes by fluorescence correlation spectroscopy. *Journal of Biological Chemistry*, *278*(30), 28109–28115. https://doi.org/10.1074/jbc.M302969200

Karp, G. (2010). Cell and Molecular Biology: Concepts and Experiments. In K. Witt, M. Staat, P. McFadden, H. Newman, A. Melhorn, & L. Muriello (Eds.), *Cell and Molecular Biology: Concepts and Experiments* (6th ed., pp. 128–136). Hoboken: John Wiley & Sons, Inc.

Keown, M. B., Ghirlando, R., Young, R. J., Beavil, a J., Owens, R. J., Perkins, S. J., … Gould, H. J. (1995). Hydrodynamic studies of a complex between the Fc fragment of human IgE and a soluble fragment of the Fc epsilon RI alpha chain. *Proceedings of the National Academy of Sciences of the United States of America*, *92*(6), 1841–5. Retrieved from http://www.pubmedcentral.nih.gov/articlerender.fcgi?artid=42378&tool=pmcentrez&rendertype=abstract

Kholodenko, B. N., Brown, G. C., & Hoek, J. B. (2000). Diffusion control of protein phosphorylation in signal transduction pathways. *The Biochemical Journal*, *350 Pt 3*, 901–7. Retrieved from http://www.pubmedcentral.nih.gov/articlerender.fcgi?artid=1221325&tool=pmcentrez&rendertype=abstract

Kinet, J.-P. (1999). THE HIGH-AFFINITY I <scp>g</scp> E RECEPTOR (FcεRI): From Physiology to Pathology. *Annual Review of Immunology*, *17*(1), 931–972. https://doi.org/10.1146/annurev.immunol.17.1.931

Kraft, S., & Kinet, J. P. (2007). New developments in FcεRI regulation, function and inhibition.

Nature Reviews Immunology, *7*(5), 365–378. https://doi.org/10.1038/nri2072

Lange, Y., Swaisgood, M. H., Ramos, B. V., & Steck, T. L. (1989). Plasma membranes contain half the phospholipid and 90% of the cholesterol and sphingomyelin in cultured human fibroblasts. *Journal of Biological Chemistry*, *264*(7), 3786–3793.

Lee, G. M., Zhang, F., Ishihara, A., McNeil, C. L., & Jacobson, K. A. (1993). Unconfined lateral diffusion and an estimate of pericellular matrix viscosity revealed by measuring the mobility of gold-tagged lipids. *Journal of Cell Biology*, *120*(1), 25–36. https://doi.org/10.1083/jcb.120.1.25

Lenne, P. F., Wawrezinieck, L., Conchonaud, F., Wurtz, O., Boned, A., Guo, X. J., … Marguet, D. (2006). Dynamic molecular confinement in the plasma membrane by microdomains and the cytoskeleton meshwork. *EMBO Journal*, *25*(14), 3245–3256. https://doi.org/10.1038/sj.emboj.7601214

Levental, I., Lingwood, D., Grzybek, M., Coskun, U., & Simons, K. (2010). Palmitoylation regulates raft affinity for the majority of integral raft proteins. *Proceedings of the National Academy of Sciences*, *107*(51), 22050–22054. https://doi.org/10.1073/pnas.1016184107

Liu, S. L., Sheng, R., Jung, J. H., Wang, L., Stec, E., O'Connor, M. J., … Cho, W. (2017). Orthogonal lipid sensors identify transbilayer asymmetry of plasma membrane cholesterol. *Nature Chemical Biology*, *13*(3), 268–274. https://doi.org/10.1038/nchembio.2268

Marquardt, D., Geier, B., & Pabst, G. (2015). Asymmetric lipid membranes: Towards more realistic model systems. *Membranes*, *5*(2), 180–196. https://doi.org/10.3390/membranes5020180

Massey, J. B., & Pownall, H. J. (2005). The polar nature of 7-ketocholesterol determines its location within membrane domains and the kinetics of membrane microsolubilization by

apolipoprotein AI. *Biochemistry*, *44*(30), 10423-10433.

Mayor, S., & Rao, M. (2004). Rafts: Scale-dependent, active lipid organization at the cell surface. *Traffic*, *5*(4), 231–240. https://doi.org/10.1111/j.1600-0854.2004.00172.x

Meer, G. van, Voelker, D. R., & Feigenson, G. W. (2008). Membrane lipids: where they are and how they behave. *Nature Reviews Molecular Cell Biology*, 112–124. https://doi.org/10.1038/nrm2330

Megha, & London, E. (2004). Ceramide selectively displaces cholesterol from ordered lipid domains (rafts): Implications for lipid raft structure and function. *Journal of Biological Chemistry*, *279*(11), 9997–10004. https://doi.org/10.1074/jbc.M309992200

Munro, S. (2003). Lipid Rafts: Elusive or Illusive? *Cell*, *115*(4), 377–388. https://doi.org/10.1016/S0092-8674(03)00882-1

OHTANI, Y., IRIE, T., UEKAMA, K., FUKUNAGA, K., & PITHA, J. (1989). Differential effects of α-, β- and γ-cyclodextrins on human erythrocytes. *European Journal of Biochemistry*, *186*(1–2), 17–22. https://doi.org/10.1111/j.1432-1033.1989.tb15171.x

Okazaki, T., Bell, R. M., & Hannun, Y. A. (1989). Sphingomyelin turnover induced by vitamin D3 in HL-60 cells. Role in cell differentiation. *The Journal of Biological Chemistry*, *264*(32), 19076–80. Retrieved from http://www.ncbi.nlm.nih.gov/pubmed/2808413

Owen, D. M., Williamson, D. J., Magenau, A., & Gaus, K. (2012). Sub-resolution lipid domains exist in the plasma membrane and regulate protein diffusion and distribution. *Nature Communications*, *3*, 1256–1258. https://doi.org/10.1038/ncomms2273

Pasenkiewicz-Gierula, M., Subczynski, W. K., & Kusumi, A. (1991). Influence of phospholipid unsaturation on the cholesterol distribution in membranes. *Biochimie*, *73*(10), 1311-1316.

Pencer, J., Jackson, A., Kučerka, N., Nieh, M. P., & Katsaras, J. (2008). The influence of

curvature on membrane domains. *European Biophysics Journal*, *37*(5), 665–671. https://doi.org/10.1007/s00249-008-0304-1

Pierini, L., Holowka, D., & Baird, B. (1996). FcεRI-mediated association of 6-μm beads with RBL-2H3 mast cells results in exclusion of signaling proteins from the forming phagosome and abrogation of normal downstream signaling. *Journal of Cell Biology*, *134*(6), 1427–1439. https://doi.org/10.1083/jcb.134.6.1427

Pike, L. J. (2006). Rafts defined: a report on the Keystone symposium on lipid rafts and cell function. *Journal of Lipid Research*, *47*(7), 1597–1598. https://doi.org/10.1194/jlr.E600002-JLR200

Putzel, G. G., & Schick, M. (2008). Phase behavior of a model bilayer membrane with coupled leaves. *Biophysical Journal*, *94*(3), 869–877. https://doi.org/10.1529/biophysj.107.116251

Pyenta, P. S., Holowka, D., & Baird, B. (2001). Cross-correlation analysis of inner-leaflet-anchored green fluorescent protein co-redistributed with IgE receptors and outer leaflet lipid raft components. *Biophysical Journal*, *80*(5), 2120–2132. https://doi.org/10.1016/S0006-3495(01)76185-1

Rentero, C., Zech, T., Quinn, C. M., Engelhardt, K., Williamson, D., Grewal, T., … Gaus, K. (2008). Functional implications of plasma membrane condensation for T cell activation. *PLoS ONE*, *3*(5). https://doi.org/10.1371/journal.pone.0002262

SANKARAN, J. (2012). *IMAGING FLUORESCENCE CORRELATION SPECTROSCOPY: THEORY, SIMULATIONS AND APPLICATIONS TO PROBE LIPID-MEMBRANE DYNAMICS* (Doctoral dissertation).

Sheets, E. D., Holowka, D., & Baird, B. (1999). Fc ♪ RI and Their Association with Detergent-resistant Membranes, *145*(4), 877–887.

Shelby, S. A., Veatch, S. L., Holowka, D. A., & Baird, B. A. (2016). Functional nanoscale coupling of Lyn kinase with IgE-FcεRI is restricted by the actin cytoskeleton in early antigen-stimulated signaling. *Molecular biology of the cell*, *27*(22), 3645-3658.

Singer, A. S. J., & Nicolson, G. L. (2017). The Fluid Mosaic Model of the Structure of Cell Membranes Published by : American Association for the Advancement of Science Stable URL : http://www.jstor.org/stable/1733071 REFERENCES Linked references are available on JSTOR for this article : You may ne, *175*(4023), 720–731.

Sonnleitner, A., Schütz, G. J., & Schmidt, T. (1999). Free Brownian motion of individual lipid molecules in biomembranes. *Biophysical Journal*, *77*(5), 2638–2642. https://doi.org/10.1016/S0006-3495(99)77097-9

Stone, M. B., Shelby, S. A., Nńñez, M. F., Wisser, K., & Veatch, S. L. (2017). Protein sorting by lipid phase-like domains supports emergent signaling function in b lymphocyte plasma membranes. *eLife*, *6*, 1–33. https://doi.org/10.7554/eLife.19891

Subczynski, W. K., & Kusumi, A. (2003). Dynamics of raft molecules in the cell and artificial membranes: Approaches by pulse EPR spin labeling and single molecule optical microscopy. *Biochimica et Biophysica Acta - Biomembranes*, *1610*(2), 231–243. https://doi.org/10.1016/S0005-2736(03)00021-X

Subramanian, K., Holowka, D., Baird, B., & Goldstein, B. (1996). The Fc segment of IgE influences the kinetics of dissociation of a symmetrical bivalent ligand from cyclic dimeric complexes. *Biochemistry*, *35*(17), 5518-5527

Vila, A., Korytowski, W., & Girotti, A. W. (2001). Spontaneous intermembrane transfer of various cholesterol-derived hydroperoxide species: kinetic studies with model membranes and cells. *Biochemistry*, *40*(48), 14715-14726.

Vist, M. R., & Davis, J. H. (1990). Phase Equilibria of

Cholesterol/Dipalmitoylphosphatidylcholine Mixtures: 2H Nuclear Magnetic Resonance and Differential Scanning Calorimetry. *Biochemistry*, *29*(2), 451–464. https://doi.org/10.1021/bi00454a021

Wawrezinieck, L., Rigneault, H., Marguet, D., & Lenne, P. F. (2005). Fluorescence correlation spectroscopy diffusion laws to probe the submicron cell membrane organization. *Biophysical Journal*, *89*(6), 4029–4042. https://doi.org/10.1529/biophysj.105.067959

Wu, M., Holowka, D., Craighead, H. G., & Baird, B. (2004). Visualization of plasma membrane compartmentalization with patterned lipid bilayers. *Proceedings of the National Academy of Sciences*, *101*(38), 13798–13803. https://doi.org/10.1073/pnas.0403835101

Xiang, Z., Block, M., Löfman, C., & Nilsson, G. (2001). Ige-mediated mast cell degranulation and recovery monitored by time-lapse photography. *Journal of Allergy and Clinical Immunology*, *108*(1), 116–121. https://doi.org/10.1067/mai.2001.116124

Young, R. M., Holowka, D., & Baird, B. (2003). A lipid raft environment enhances Lyn kinase activity by protecting the active site tyrosine from dephosphorylation. *Journal of Biological Chemistry*, *278*(23), 20746–20752. https://doi.org/10.1074/jbc.M211402200

INDEX

G

H

I

K

L

M

N

O

P

R

S

T

U

V

W

Y